218
1-19-77

Dr 634

UCRL-52133

PARTICLE-IN-CELL VS STRAIGHT-LINE AIRFLOW GAUSSIAN CALCULATIONS OF CONCENTRATION AND DEPOSITION OF AIRBORNE EMISSIONS OUT TO 70 KM FOR TWO SITES OF DIFFERING METEOROLOGICAL AND TOPOGRAPHICAL CHARACTER

R. Lange
M. A. Dickerson
K. R. Peterson
C. A. Sherman
T. J. Sullivan

October 8, 1976

Prepared for U.S. Energy Research & Development Administration under contract No. W-7405-Eng-48

Printed in the United States of America
Available from
National Technical Information Service
U.S. Department of Commerce
5285 Port Royal Road
Springfield, VA 22161
Price: Printed Copy $; Microfiche $3.00

Page Range	Domestic Price	Page Range	Domestic Price
001-025	$ 3.50	326-350	10.00
026-050	4.00	351-375	10.50
051-075	4.50	376-400	10.75
076-100	5.00	401-425	11.00
101-125	5.50	426-450	11.75
126-150	6.00	451-475	12.00
151-175	6.75	476-500	12.50
176-200	7.50	501-525	12.75
201-225	7.75	526-550	13.00
226-250	8.00	551-575	13.50
251-275	9.00	576-600	13.75
276-300	9.25	601-up	*
301-325	9.75		

*Add $2.50 for each additional 100 page increment from 601 to 1,000 pages; add $4.50 for each additional 100 page increment over 1,000 pages.

Distribution Category
UC-11

LAWRENCE LIVERMORE LABORATORY
University of California Livermore, California 94550

UCRL-52133

PARTICLE-IN-CELL VS STRAIGHT-LINE AIRFLOW GAUSSIAN CALCULATIONS OF CONCENTRATION AND DEPOSITION OF AIRBORNE EMISSIONS OUT TO 70 KM FOR TWO SITES OF DIFFERING METEOROLOGICAL AND TOPOGRAPHICAL CHARACTER

R. Lange, M. H. Dickerson, K. R. Peterson,
C. A. Sherman, and T. J. Sullivan

MS. date: October 8, 1976

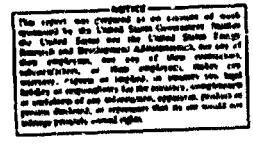

Contents

Abstract 1
I. Introduction 1
II. Model Discussion 2
III. Model Input Data 7
IV. Model Calculations 18
V. Comparison of Results of Particle-in-Cell Model and Gaussian Model . . 32
VI. Conclusions and Recommendations 60
Acknowledgment 60
References 61
Appendix A: Comparison of ADPIC and Gaussian Plume Depletion Factors . . 63
Appendix B: Input Meteorological Parameters 65

PARTICLE-IN-CELL VS STRAIGHT-LINE AIRFLOW GAUSSIAN CALCULATIONS OF CONCENTRATION AND DEPOSITION OF AIRBORNE EMISSIONS OUT TO 70 KM FOR TWO SITES OF DIFFERING METEOROLOGICAL AND TOPOGRAPHICAL CHARACTER

Abstract

Two numerical models for the calculation of air concentration and ground deposition of airborne effluent releases are compared. The Particle-in-Cell (PIC) model and the Straight-Line Airflow Gaussian model were used for the simulation. Two sites were selected for comparison: the Hudson River Valley, New York, and the area around the Savannah River Plant, South Carolina. Input for the models was synthesized from meteorological data gathered in previous studies by various investigators. It was found that the PIC model more closely simulated the three-dimensional effects of the meteorology and topography. Overall, the Gaussian model calculated higher concentrations under stable conditions with better agreement between the two methods during neutral to unstable conditions. In addition, because of its consideration of exposure from the returning plume after flow reversal, the PIC model calculated air concentrations over larger areas than did the Gaussian model.

I. Introduction

The U.S. Nuclear Regulatory Commission (NRC) regulation 10CFR Part 50, Appendix I provides numerical guides for design objectives and limiting conditions of radioactive effluent criteria that must be met by designers and operators of light-water-cooled nuclear power plants. To implement Appendix I, several acceptable methods for calculating effluent releases, dispersion of the effluent in the atmosphere and in water bodies, and radioactive doses have been developed by the NRC staff. For a routine airborne release, the concentration of radioactive material in the surrounding region depends on the amount of effluent released; the height of the release; the momentum and buoyancy of the emitted plume; the windspeed, atmospheric stability, and airflow patterns of the site; and various effluent removal mechanisms. Geographical features such as hills,

valleys, and large bodies of water greatly influence dispersion and airflow patterns.

In Regulatory Guide 1.111,[1] the NRC staff lists three general atmospheric transport and diffusion models that are acceptable for assessing potential annual radiation doses to the public from routine releases of radioactive materials in gaseous effluents. These models are Particle-in-Cell (PIC), Segmented-Plume, and Straight-Line Airflow. Except for those cases in which the license applicant or licensee proposes an acceptable alternative method, the methods described in this regulatory guide will be used until revisions are made.

In this study, we analyzed the differences between calculations of air concentration and ground deposition for the Straight-Line Airflow Gaussian Model and the PIC model, using two typical geographical locations in the U.S. The PIC model used in this study is the Atmospheric Diffusion Particle-in-Cell (ADPIC) computer code. A similar study by Van der Hoven et al.[2] compared the Segmented-Plume Model to the Straight-Line Airflow model.

We chose the Hudson River Valley and an area in the Southeastern U.S. for the numerical simulation and comparisons. For these sites, we synthesized a regional, 24-h cyclic wind field (70-km radius from the source) using data from studies that had previous investigations of the wind-flow patterns in these areas. Because we wished to analyze the two methods for an assumed operating release of short duration in a particular meteorological regime, the meteorological data used as input for the models provided a basis for comparison. For the next phase of this study with more complex models for assessments of a year's data record, we plan to use meteorological measurements taken on-site and at surrounding National Weather Service (NWS) stations plus any other valid measurements taken in the area.

II. Model Discussion

The straight-line airflow Gaussian diffusion calculations were made with the LLL computer code CPS (continuous point source).[3] This code estimates concentrations and surface deposition from 0.1 to

100 km. It is similar in most respects to Sagendorf's model[4] and nearly all of the theory is based on Ref. (5). The basic code inputs are the atmospheric stability category and the wind speed. However, a number of refinements are included such as wind speed as a function of height, enhanced dilution from building wakes near the source, calculation of plume center trajectory as a function of effluent heat flux and wind speed, physical stack height, topography as a function of distance from source, dry deposition due to turbulent processes, wet deposition due to precipitation, radioactive decay, nonzero background for the particular effluent involved, and whether the release was routine or accidental. The code either outputs the concentration calculations as a function of distance from one set of meteorological data or stores information from many meteorological data sets. From these data, it prepares contour plots as a function of azimuth for 16 sectors and as a function of distance of both average concentrations and concentrations at different probability levels.

PIC Model Components

The PIC model components and the input information required to calculate integrated air concentrations and ground deposition from time- and space-varying meteorological input data are depicted in Fig. II-1. MATHEW[6,7] is a meteorological adjustment model developed to provide the diffusion and transport model, ADPIC,[8,9] with mass-consistent, three-dimensional input wind fields. These wind fields are adjusted by a weighted least squares to satisfy the continuity equation within the specified volume. The upper and lateral boundaries are assumed to be open air, thus allowing mass to flow through these boundaries. The bottom boundary is determined by the topographic elevations of the area of interest. The observed data needed for the adjustment are provided within the code by an interpolation-extrapolation scheme. This scheme uses information available at a given site to determine the observed horizontal velocity component at each grid point above the topography.

[4] The most significant difference between the models involves input format. The CPS code uses a separate punch card for each average hourly observation of wind and stability. Calculations are made sequentially and accumulated. Concentration and deposition sums are divided by the total number of observations within each section. However, Sagendorf's model inputs joint frequency distributions of wind and stability that have been prepared previously.

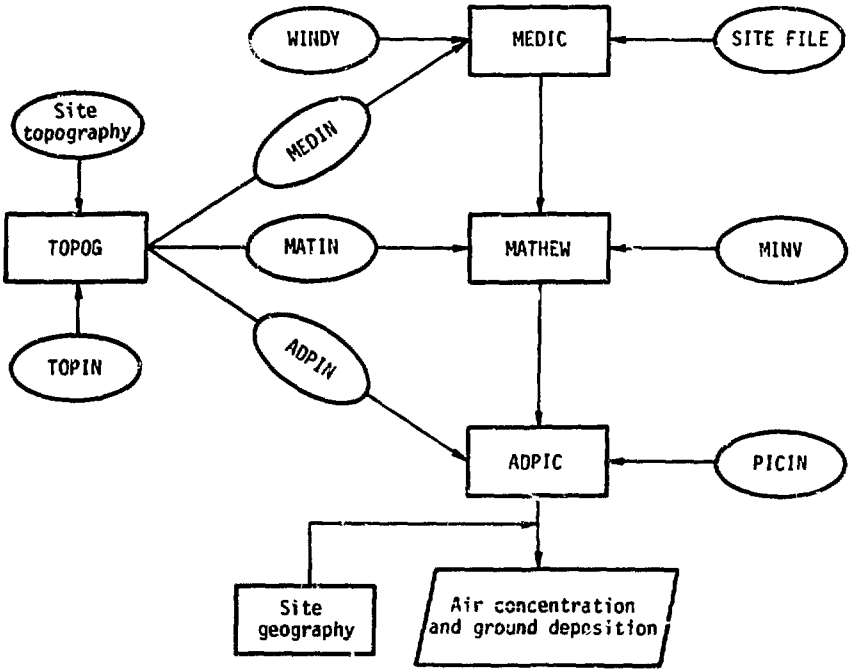

Fig. II-1. Schematic diagram of model components for the PIC method.

These observed velocities are assumed to be a fair and reasonable representation of the actual wind field and need only to be minimally adjusted to significantly reduce the remaining divergence.

ADPIC is a hybrid Lagrangian-Eulerian, three-dimensional particle-in-cell code for calculating transport and diffusion of a pollutant from its source to its temporal and regional distribution. This numerical model can simulate transport and diffusion when given speed and directional wind shear, occurrence of calms, space-variable surface roughness, wet and dry deposition, radioactive decay, gravitational settling, space- and time-dependent eddy diffusion parameters, and single or multiple sources of either a continuous or instantaneous nature. ADPIC solves the three-

dimensional, advection-diffusion equation in a flux-conservative form, using a pseudovelocity technique with the advective wind supplied by MATHEW.

Here, the Lagrangian particles represent the activity distribution and the concentration associated with the aerosol within the structure of an Eulerian grid. The chief advantages of this approach are the virtual elimination of artificial diffusion that is inherent in purely Eulerian, finite difference codes and the fact that the Lagrangian particles can be tagged with their coordinates, mass or size distribution, activity, age, and other properties that might be exhibited by a particular pollutant.

MEDIC is a meteorological data interpolation computer code used to interpolate horizontal wind measurements to grid points at a fixed height above topography. WINDY is an input file that contains the horizontal winds and temperatures measured locally at the site in addition to measurements in the surrounding area reported by NWS and other sources. The SITE FILE supplies the coordinate location of the meteorological measurements. New WINDY files can be compiled as often as additional meteorological information becomes available.

Output from MEDIC is used by MATHEW to calculate a three-dimensional nondivergent regional windfield. MINV and PICIN are site specific input files that are generated each time the conditions at a specific site change. For example, PICIN furnishes ADPIC with information related to the source term (e.g., height above topography, constituents, buoyancy, and strength if known). In case the source term is not known, ADPIC can assume a unit rate release and, if the release rate is relatively uniform, the final calculations can be adjusted with estimates of the source-term strength. Thus, in its present form, ADPIC can simulate five different species emitted from one location, one species emitted from five locations, or any combination of species and release points that total five in number. Because we wanted to simulate both noble gases and gases that exhibit a deposition velocity, each with a different half-life, this feature was extremely useful.

TOPOG is used to set up the MEDIN, MATIN, and ADPIN input files that contain topographical and geographical coordinates for MEDIC, MATHEW, and ADPIC, respectively Because it is unlikely that an entire region for which we have topography will be required for any one calculation, TOPOG selects the topography

of interest from the site topography data base and the grid origins for the three computer codes. In addition, TOPOG calculates the topographic boundary conditions for MATHEW and ADPIC.

Verification of Computer Codes

ADPIC has undergone extensive verification against closed solutions to the transport and diffusion equation.[9] In these studies we found that ADPIC results are within 5% of the exact solution for uniform flow fields as well as for wind fields that exhibit vertical wind shear. ADPIC has also been used for plume depletion studies over agricultural land under simple meteorological conditions.[10] For this study, we have made a consistent comparison between ADPIC and our Gaussian CPS code of plume depletion factors over agricultural land for a 10-m release height and for both an F and a B Pasquill stability regime. These results are shown in Appendix A.

The MATHEW-ADPIC computer codes have been verified against several field tracer studies.[11] These studies included methyl-iodine tracer studies at the Idaho National Engineering Laboratory, Idaho, and ^{41}Ar plumes at the Savannah River Plant (SRP), South Carolina. For these studies, the agreement between measurements and calculations has been remarkably consistent; 60% of the calculations are within a factor of two. Measurements were taken at distances of 4 to 80 km from the source and have included high-volume surface samples for the methyl-iodine as well as surface and airborne measurements of gamma energy from ^{41}Ar.

Recently, we conducted another series of simultaneous ^{41}Ar and SF_6 tracer experiments at the SRP in conjunction with the Savannah River Laboratory (SRL) personnel. Although a detailed comparison of measurements and calculations has not yet been completed, preliminary results indicate that the MATHEW-ADPIC computer codes were able to successfully calculate concentrations during a 180° shift in wind direction for a 4-h SF_6 release.

These computer codes were originally interfaced to support real-time calculations for the Atmospheric Release Advisory Capability (ARAC) project and thus, we had to make several modifications to run them in a production mode for this study. These modifications were not extensive and did not require any major changes to the codes themselves or to the input files. We did not run these computer codes in their operational mode, straight through from MEDIC to the end of the ADPIC calculations. Instead, we ran them

separately so that output from MEDIC could be evaluated to ensure that the interpolated wind fields over the topography were consistent with the input wind observations. After these wind fields were verified, we ran all the data sets through MATHEW and the adjusted wind fields were analyzed for consistency. Finally, the adjusted wind fields were used in the ADPIC code to calculate time-integrated air concentration and ground deposition. By running the codes in this mode, we felt more confident that the calculations would be consistent with the input data and with the assumptions used for the source terms.

III. Model Input Data

Topographic data bases for this study were obtained by averaging fine-resolution elevations supplied by the U.S. Geological Survey for the two areas of interest.

The model-generated topography for the Hudson River Valley calculation consists of a narrow river valley in the north end of the grid with high topography in the west and lower hills toward the east (Fig. III-1). The river narrows into a gorge and turns east-northeast through a southwest – northeast ridge, 200 to 300 m in height. Once through the ridge, the river turns abruptly southwest and begins widening as the topography drops and becomes more rolling, particularly to the east. About midway south in the grid, the river turns southeast at the head of a widening flood plain that is interrupted by a narrow rise (40 to 80 m) trending north-south. An elevated plateau extends along the southwestern side of the mesh. The river turns south near the east boundary of the grid, about two-thirds of the distance from the north boundary, and proceeds south out of the grid. The source release point is slightly southeast of the river gorge, as indicated by the solid circle in Fig. III-1.

The meteorology of the Hudson River Valley site was studied using 2 y of observations at the site itself and in surrounding locations.[13] It was found that, frequently, diurnal valley winds blow up and down the axis of the river valley (up-valley during unstable hours and down-valley during stable hours). In general, these local winds are most frequent under clear skies and relatively light prevailing winds occur in the autumn. In Figs. III-2 and III-3, we show the diurnal vector mean wind as measured 21 m

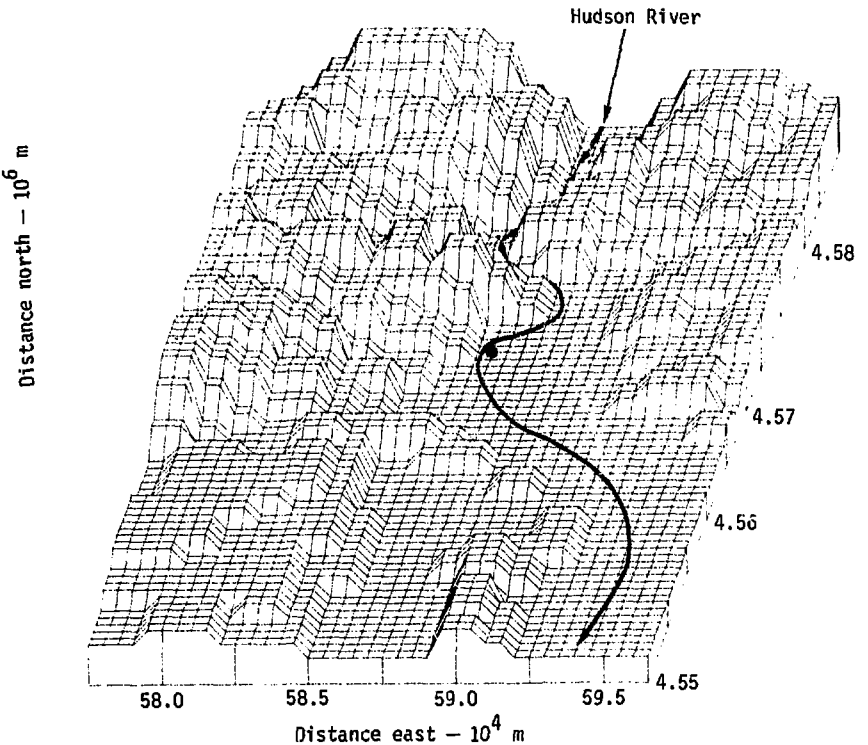

Fig. III-1. Computer generated topography (MATHEW) for the Hudson River Valley. Source is located by (●).

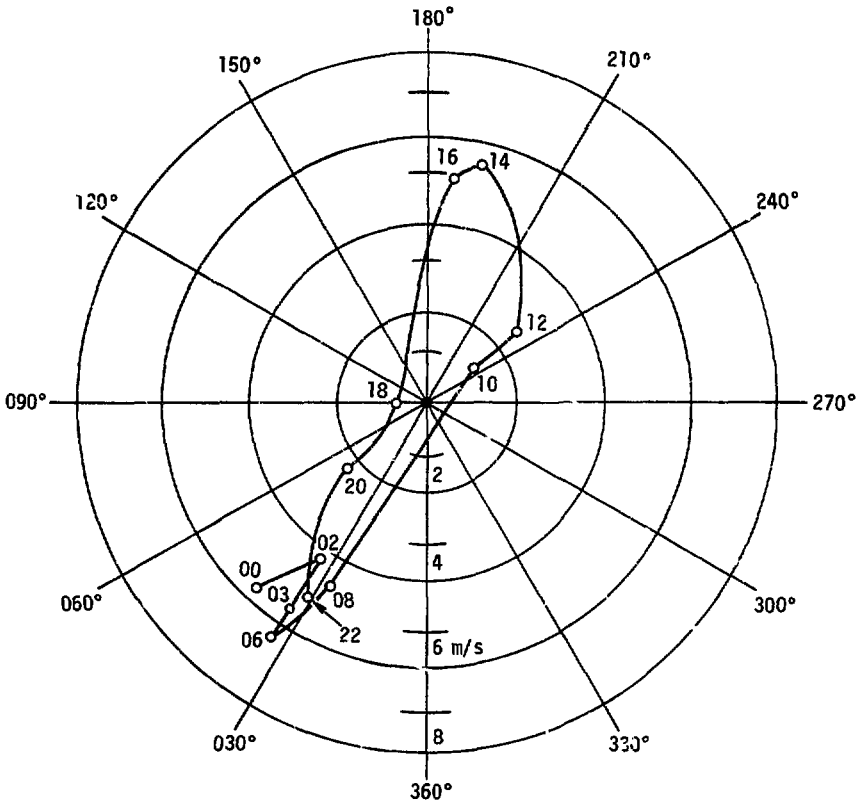

Fig. III-2. Diurnal-variation hodograph of the mean vector wind speed at Hudson River Valley for pressure-gradient conditions of virtually zero. September through October 1955, 21 m above the Hudson River beginning at midnight (00 h), EST.

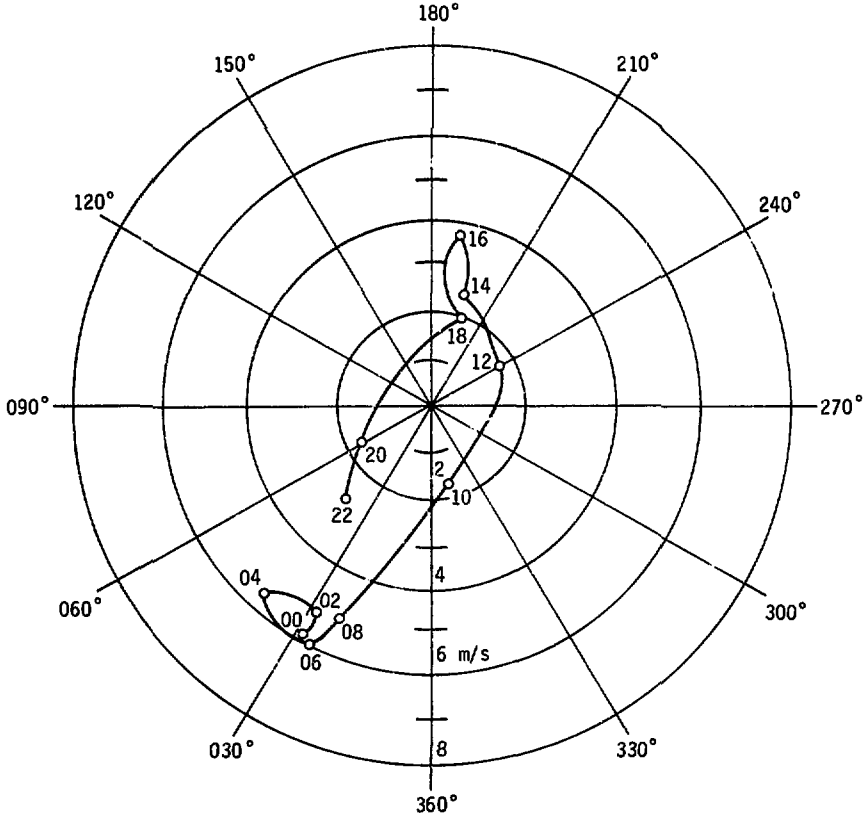

Fig. III-3. Diurnal-variation hodograph of the mean vector wind at Hudson River Valley for 24-h periods of weak pressure-gradient conditions (geostrophic winds less than 7 m/s), September through October 1955, 21 m above the Hudson River beginning at midnight (00 h) EST.

above the river during September through October 1955 (all times are local EST). Figure III-4, a plot of the ratio of the mean vector to the mean scalar speed as a function of local time and the strength of the prevailing flow, shows the steadiness of the wind in autumn. We used this information to estimate the Pasquill diffusivity categories as a function of the time of day. During transition periods when the flow is reversing, the horizontal diffusion coefficients are larger than during either an up-valley or a down-valley flow. For the vertical diffusion coefficients, we used a stable regime for the nighttime flow conditions, moving into an unstable regime during the daytime hours.

With these conditions, we simulated a cyclic flow reversal in the Hudson River Valley for an

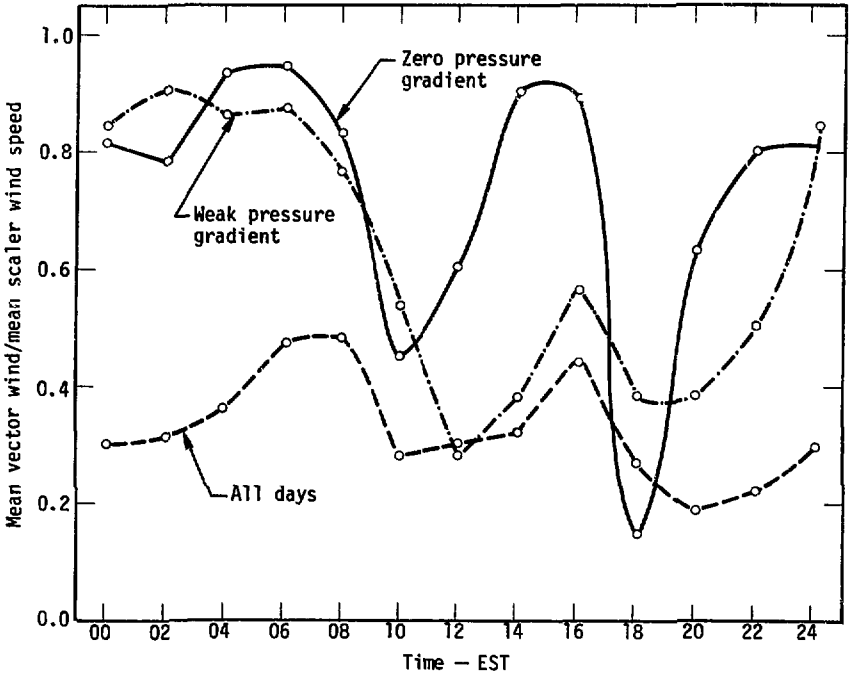

Fig. III-4. Steadiness of wind (mean-vector wind speed/mean-scalar wind speed) vs time of day for indicated pressure-gradient conditions.[13]

early fall, clear weather situation (Fig. III-5). The general flow is characterized by thermally driven currents at the lowest levels with a south to southwesterly flow prevailing above the boundary layer. The nighttime cycle consists of 14 h of very light (0.25 to 0.5 m/s) northerly flow, gradually increasing to an average of 2.5 m/s as the cool, very stable wedge of drainage air deepens from 20 to 120 m. The daytime cycle

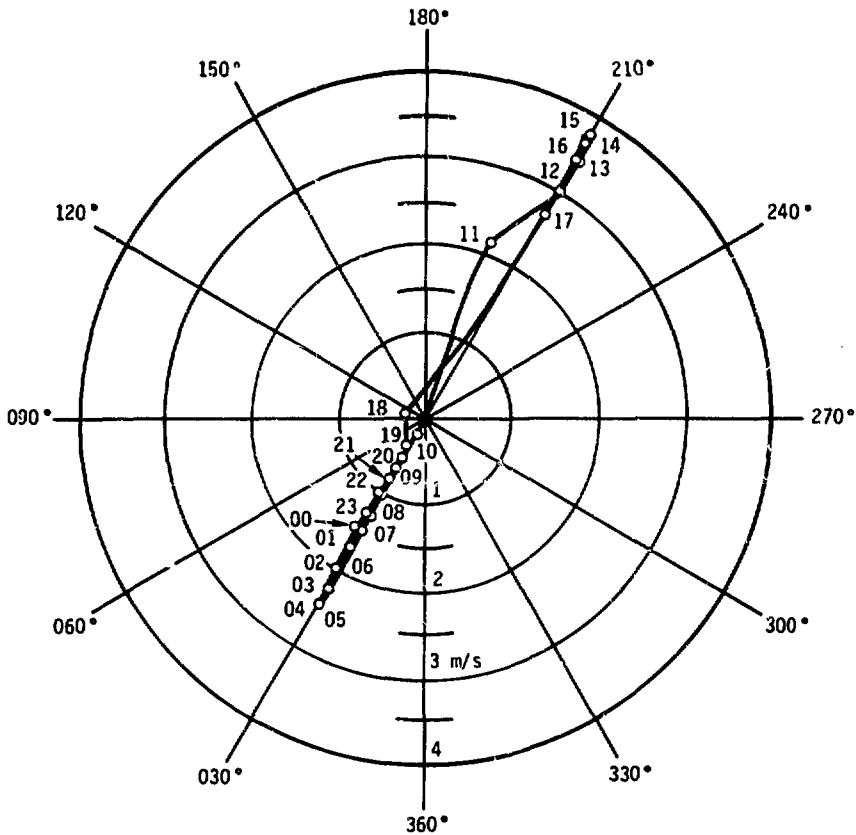

Fig. III-5. Assumed variation of mean wind-vector speed (m/s) for a 24-h period in the Hudson River Valley.

consists of a sudden late morning decrease in stability, changing to neutral, to slightly unstable, and then to moderately unstable with a concomitant breaking up of the thermal inversion, a rapid deepening of the boundary layer, and a quick rise of the southerly wind. An average southerly wind of 3.8 m/s develops for about 6 h with a 2.5 m/s flow existing for 1 h on either end of the cycle. During dawn and dusk transition cycles, the wind speeds generally reflect a light and variable condition. Figure III-6 shows the variation of the inversion height and the mean wind speed as a function of the local time assumed for the calculations in the following section. To simulate the flow regime over the region, we postulated bogus stations throughout the grid where we input winds that are consistent with the topography and the meteorological conditions under consideration. A tabular listing of these input winds is presented in Appendix B.

For a typical area in the southeastern U.S., we selected the area around the Savannah River Plant in Aiken, South Carolina. This area was chosen because LLL has been engaged in studies related to the ARAC project with the SRL personnel for the

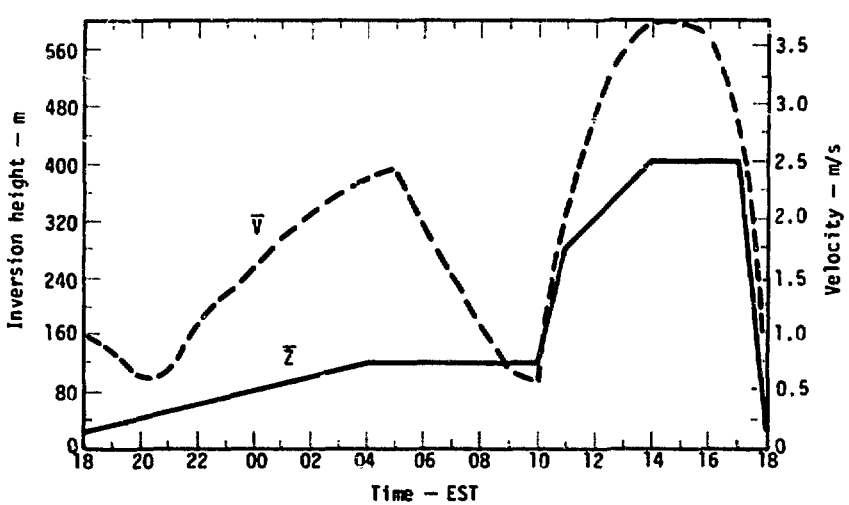

Fig. III-6. Assumed variation of mean wind speed ($\bar{V}$) and height of inversion base ($\bar{Z}$) vs time of day for the Hudson River Valley.

past several years. During this time, a number of real-time transport and diffusion experiments have been conducted; measurements of ^{41}Ar were made over SRP and calculations were performed at LLL. Thus, the topography for the area surrounding the SRP and the locations of the wind reporting stations were already available.

Model topography for this area consists of a slightly undulating plane inclined from northwest to southeast with a few slightly eroded, relatively straight river channels of moderate width (Fig. III-7). No abrupt topographic barriers are evident nor are there any dominant channeling features except for the most stable drainage flow down the

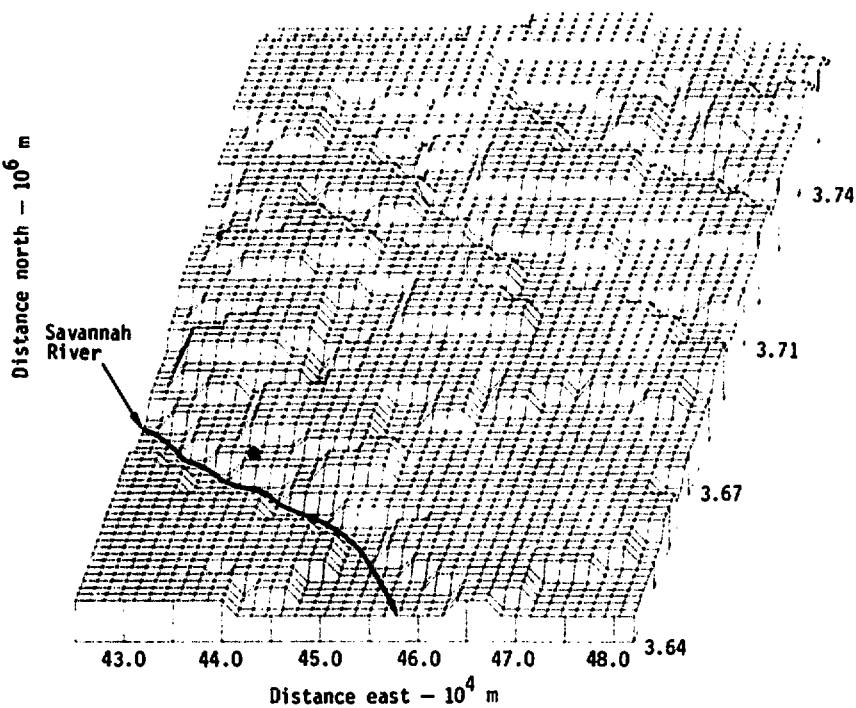

Fig. III-7. Computer generated topography (MATHEW) for the area around the Savannah River Plant. Source is located by (●).

river channels. The release point is in the southwestern portion of the model grid as indicated by a solid circle in Fig. III-7.

The basic meteorological regime chosen here is characterized by an average late summer condition prevalent in the southeast; a south to south-southwesterly flow aloft and at the surface during the day.[14] At night, a very shallow stable layer develops, not exceeding 70 m in depth while highly variable, light drainage winds gradually develop into a general northwesterly trend out of the slowly diminishing south-southwest flow. In mid-morning the stable layer inversion is quickly dissipated, the boundary layer rapidly deepens to the 400-m depth of the grid domain, and concurrently the stability cycles from stable to moderately unstable. The daytime surface winds rotate from generally north-northwest to southeast and then settle into a prevailing southerly direction with speeds averaging 4.6 m/s. The diurnal variation of the winds used for this area is shown in Fig. III-8. This flow pattern is considerably different from the pattern shown for the Hudson River Valley, an area that exhibits significant topographical influences. Figure III-9 shows the mean wind speed and inversion height vs time of day that were used for the southeastern U.S. simulation.

As for the Hudson River Valley flow problem, the wind condition over the SRP area were taken from the postulated wind reporting stations around the area. The meteorological data used in this study are also listed in Appendix B.

It is important to emphasize again that the meteorological data used in each of these problems are not actual measurements but are based on studies of the prevailing climatological conditions in these areas. The purpose of this study was to illustrate the differences and similarities between the traditional Gaussian calculations and a more complex numerical simulation of transport and diffusion and thus, these data only need to be a reasonable representation of conditions that frequently occur in these two areas.

In Table III-1 we have listed the five different species used in the model calculations. Four of these are radioactive isotopes, selected because of their relevance to an operating release from a nuclear power reactor. The fifth, inert gas, was chosen as a control species. All five species were run simultaneously in the ADPIC calculations and were each assumed to be unit rate releases (1 unit/s).

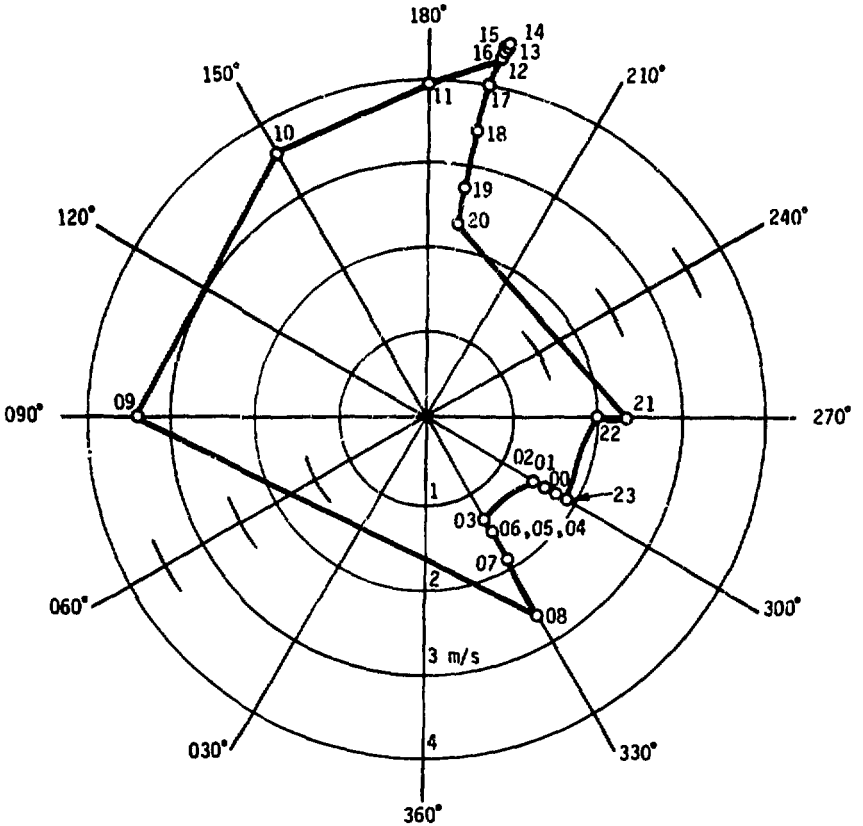

Fig. III-8. Assumed variation of mean wind-vector speed (m/s) for a 24-h period in the area around the Savannah River Plant.

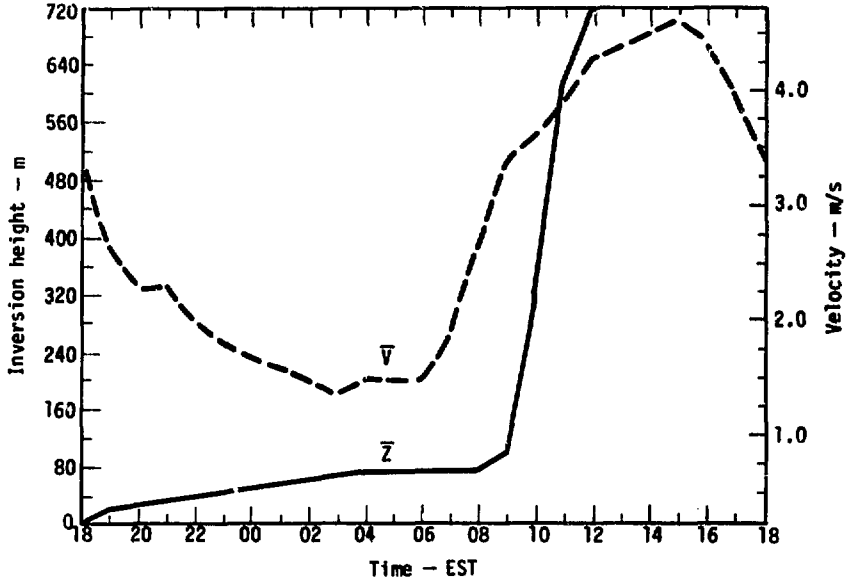

Fig. III-9. Assumed variation of mean wind speed ($\bar{V}$) and height of inversion base ($\bar{Z}$) for the area around the Savannah River Plant.

Table 3.1. Elemental species used in model calculations.

Species	Half-life (s)	Deposition velocity (m/s)
^{131}I	6.91×10^5	0.005
^{88}Kr	1.01×10^5	-
^{138}Xe	8.40×10^2	-
^{133m}Xe	2.01×10^5	-
Inert gas	∞	-

IV. Model Calculations

Selection of the MATHEW-ADPIC grids was based on a variety of conditions; limitation of computer storage size, time step considerations to minimize computer cost of running the problems, cell size requirements for the grid to resolve the pollutant cloud and topography, and sufficient extent of the grid in both the horizontal and vertical direction to retain most of the pollutant until wind reversal occurs.

For the Hudson River Valley study, the grid consisted of 38 × 78 × 10 cells of 500 × 500 × 45 m each, giving a total grid block of 19 × 39 × 0.45 km in the east-west, north-south, and vertical directions, respectively. Because the topography protrudes like building blocks into the grid, the horizontal cell size of 500 m was required to resolve the narrowest part of the river. In the vertical direction, a cell height of 45 m was chosen to give sufficient resolution to the variations in elevation associated with the river valley. Careful consideration was given to the location of the source within the grid. Because ADPIC is a time-dependent code, it was important to ensure sufficient grid space around the source to prevent a significant fraction of the pollutant from escaping the grid before wind reversal occurred and before the code could model the return of the earlier part of the plume to the source area and beyond. Preliminary computations indicated that a northerly nighttime drainage wind with F stability along the Hudson River would require about 20 km of grid south of the source to reduce (by a factor of 10^6 to 10^7) the concentration of a pollutant parcel that reached the edge of the grid and then returned to the source location. In this way, any parcel of pollutant that left the southern face of the ADPIC grid and was therefore lost from the problem would have made a negligible contribution to secondary exposure due to wind reversal. Similarly, the 450-m vertical dimension of the ADPIC grid was great enough to be above the channeling effect of the river. Under stability conditions when the mixed layer exceeded the grid height (unstable), pollutant particles lost through the top of the grid would have had a very low probability of ever contributing to a surface-air concentration.

Similar considerations for the southeastern U.S. site produced a grid of 38 × 78 × 10 cells of 1500 × 1500 × 30 m for a total grid

of 57 × 117 × 0.3 km in the east-west, north-south, and vertical directions, respectively.

The wind data tabulated in Appendix B were processed with the MEDIC and MATHEW models to produce a three-dimensional, mass-consistent advection field for 24 h for both sites. The general features of MEDIC-MATHEW adjustment can be seen through an examination of a sample data set from each site.

The "measured" horizontal wind vectors for 1200 EST in the Hudson River Valley are shown in Fig. IV-1. The resulting interpolated horizontal wind in Fig. IV-2a is shown at 90 m above the lowest topography in the grid. The horizontal isotachs are overlaid with streamlines defining the flow direction. The spacing between the streamlines is only qualitatively related to the wind speed. The blank areas in Fig. IV-2 delineate the area where the topography is higher than 90 m above the reference elevation. A comparison of the adjusted horizontal field (Fig. IV-2b) with the interpolated winds (Fig. IV-2a) shows the effect of channeling near the narrowest part of the Hudson River Valley. The streamline curvature is smoothed and shows more conformity to the terrain. The channeling has also resulted in a 2 m/s increase in a high windspeed area, located one-third of the way from the northern border of the grid. Referring to the topography of Fig. III-1, the remaining relative high speed designations are seen to be related to terrain changes. The accompanying vertical velocities for the 90-m level are shown in Fig. IV-3. While the vertical motion is relatively small at this level, it is sufficient to produce motion over the appropriate terrain features. Where the terrain is more rugged and higher, the wind fields at those levels appropriately show more vertical motion.

Although the visualizations of the interpolated and adjusted horizontal fields appear quite comparable, the root mean square (rms) change in speed and direction for grid points 90 m above topography was 0.7 m/s and 28°. Over the entire grid volume, the rms speed and direction adjustment was 0.4 m/s and 22°. Almost 20% of the grid points in the mesh are below the terrain. A full graphical portrayal of the three-dimensional field over the Hudson River is not technically feasible at present. Figure IV-4 illustrates another view of the advection field where the horizontal speed and direction are calculated at 45 m above terrain. The relative low speeds are just windward of rising terrain while the relative high

speeds occur above the flatter areas.

The 2300 EST wind field for the southeastern U.S. site includes some "measurements" just outside the calculation grid. The horizontal wind measurements falling within the grid are shown in Fig. IV-5. The influence of the remaining measurements is included in the interpolated field of Fig. IV-6a at 150 m above the

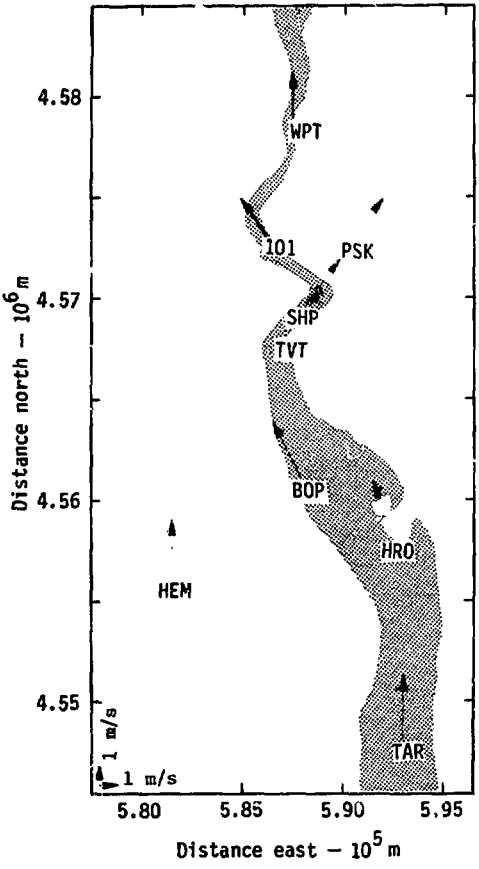

Fig. IV-1. Assumed surface-wind measurements at 1200 EST in the Hudson River Valley. Locations: BOP, Bowline Point; HEM, Hempstead; HRO, Hudson River; IOI, Iona Island; PSK, Peekskill; SHP, Ship; TAR, Tarrytown; TVT, Indian Point; WPT, West Point.

reference elevation. Most of the terrain in this area is below the 150-m level although some grid points near the northwest corner are still below the topographic elevations. The adjusted horizontal wind field of Fig. IV-6b is quite similar to the interpolated field. The major changes occur in the northeast and account for a substantial shift in wind direction. The vertical

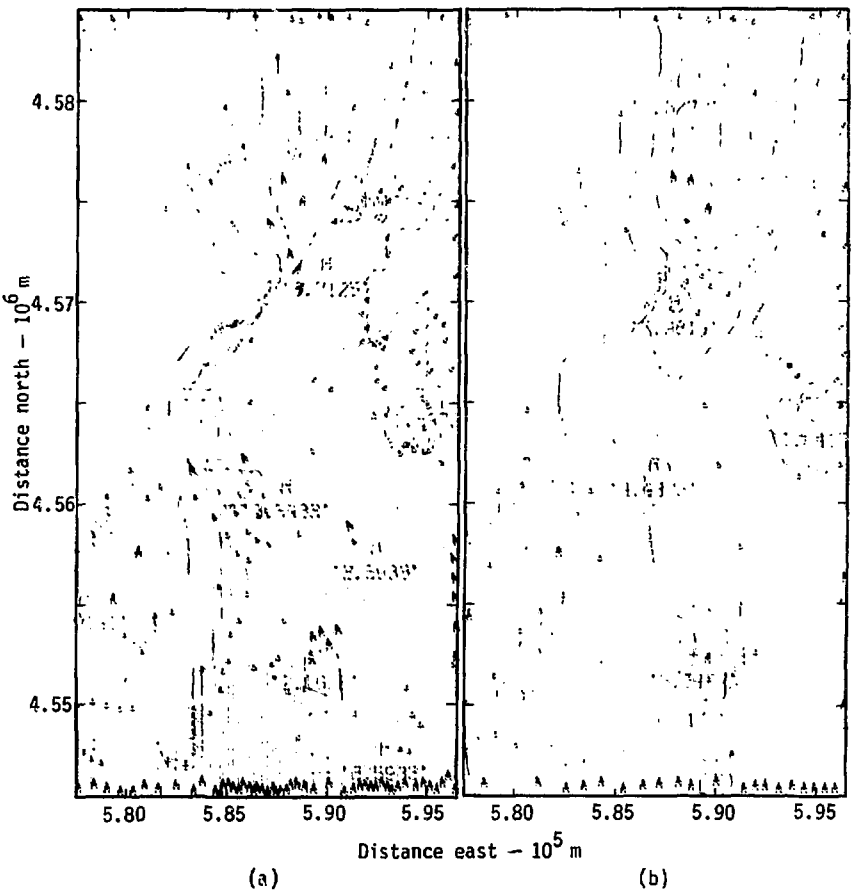

Fig. IV-2. Interpolated (a) and adjusted mass-consistent (b) horizontal wind field (m/s) at 1200 EST in the Hudson River Valley 90 m above the lowest topography in the grid.

velocity at the 150-m level, shown in Fig. IV-7, illustrates the calculated adjustment for the sloping terrain of the site. The overall wind pattern can be seen in Fig. IV-8. At 60 m above the topographic elevations, the wind-direction changes in the input data are readily seen in the adjusted field.

The rms changes for the southeastern site reflect the relative smoothness of the terrain. At the 150-m level, the rms values of wind speed and direction are 0.3 m/s

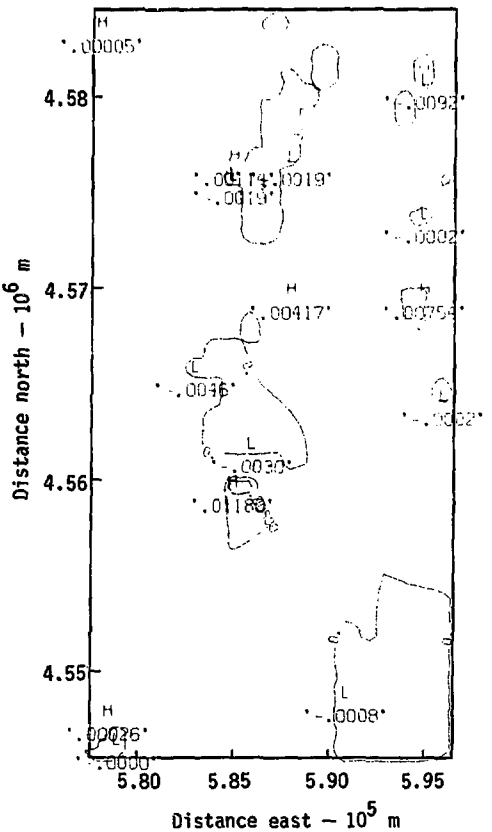

Fig. IV-3. Vertical velocity contours (m/s) at 1200 EST in the Hudson River Valley.

and 12°, respectively, while the overall rms change was 0.2 m/s in speed and 10° in direction. As in the Hudson River Valley calculation, 20% of the grid points were below the topography. The results of adjusting the remaining 23 h at each site are comparable to the two calculations shown. Speed and direction changes are appropriate to the input conditions and the terrain.

For both the Hudson River Valley and the southeastern U.S. sites, ADPIC was run for a complete 24-h

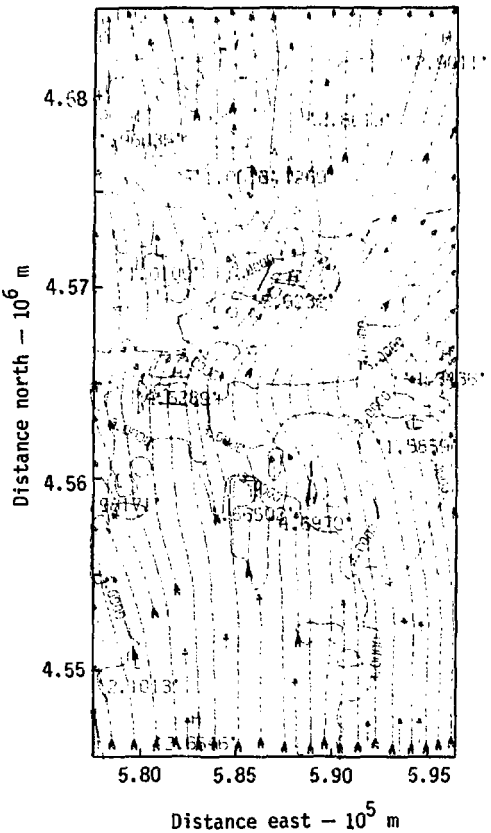

Fig. IV-4. Adjusted wind field (m/s) 45 m above the topography at 1200 EST in the Hudson River Valley.

diurnal cycle. Deposition and integrated surface air concentrations from unit rate surface releases for five typical reactor effluents were compared with results from the Gaussian model. Additionally, the Hudson River site was run for a second 24-h cycle, identical to the first, to determine the effect of the initial conditions on the 24-h concentrations. Initially, the ADPIC grid contained no pollutant. In reality, for a continuous release some background pollutant from an

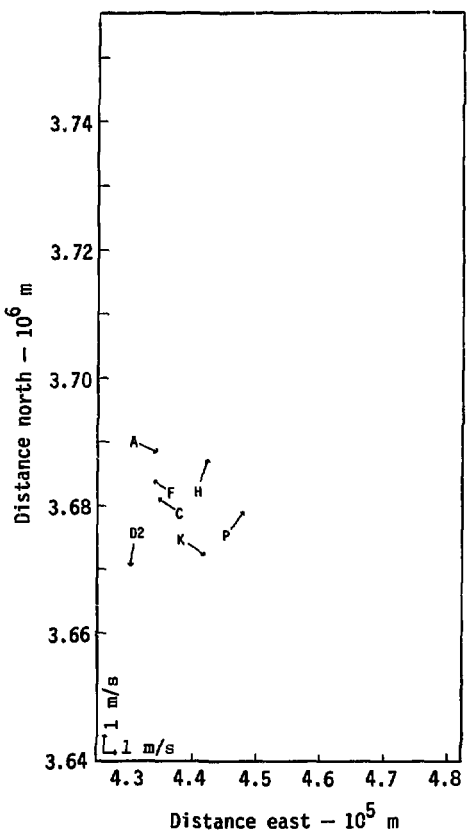

Fig. IV-5. Assumed surface wind measurements at 2300 EST in the Savannah River area. Locations: A, C, D2, F, H, K, and P; Savannah River Plant Meteorological Towers.

earlier time would be expected to be present.

The source term for both site studies consisted of a simultaneous, continuous unit rate surface release (1 unit/s of the four radioisotopes, ^{131}I, ^{133m}Xe, ^{88}Kr, and ^{138}Xe, and the inert gas control species

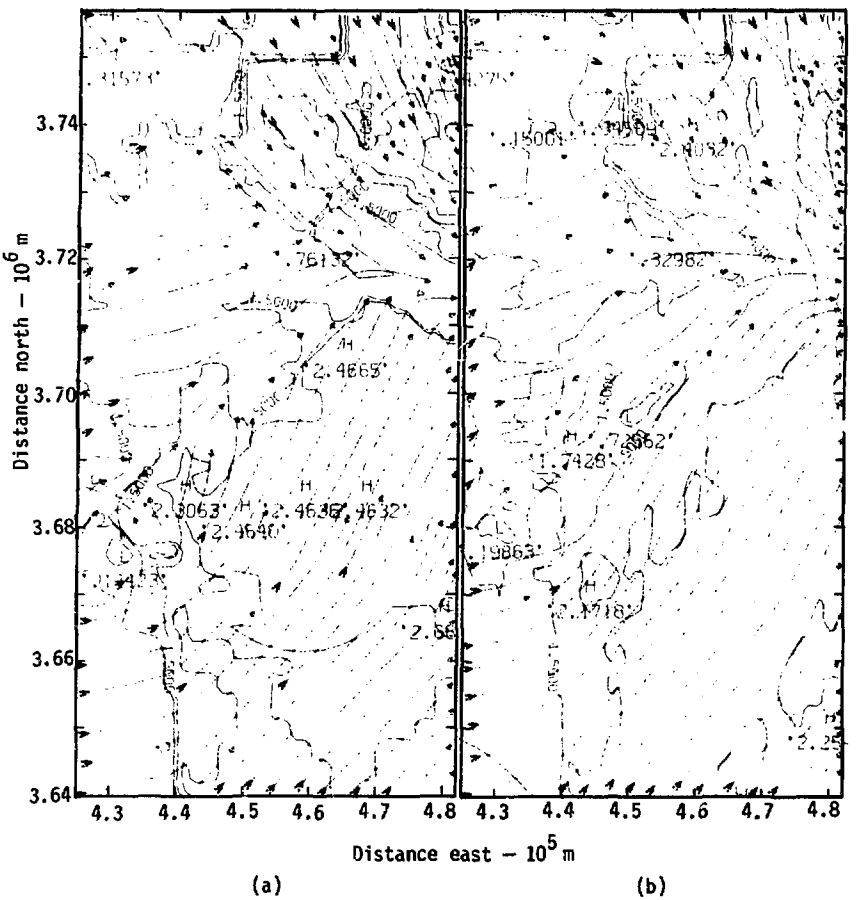

Fig. IV-6. Interpolated (a) and adjusted mass-consistent (b) horizontal wind field (m/s) at 2300 EST in the Savannah River area.

(see Table III-1). The sources were assumed to have a Gaussian distribution with a horizontal and vertical standard deviation of σ_H = 10 m and σ_V = 5 m, respectively. Source location for the Hudson River Valley was on the edge of the west bank of the river at river level height (Fig. III-1) and near the Savannah River Plant for the southeastern U.S. site (Fig. III-7).

The ADPIC code modeled the transport and diffusion of the total pollutant plume by generating some

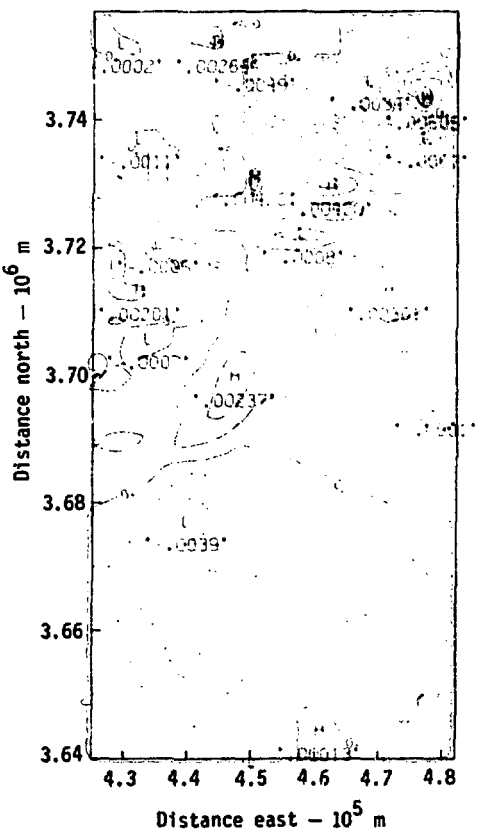

Fig. IV-7. Vertical velocity contours (m/s) at 2300 EST in the Savannah River area.

90,000 tracer particles for a typical 24-h study, of which a maximum of 20,000 resided simultaneously within the grid, the rest either being deposited, radioactively decayed, or carried out of the grid by the diffusion-advection process. The particle-in-cell approach of ADPIC also allowed the separate treatment of radioactive decay and deposition of the individual isotopes.

Figures IV-9 to IV-12 give examples of the ADPIC particle distribution, representing the

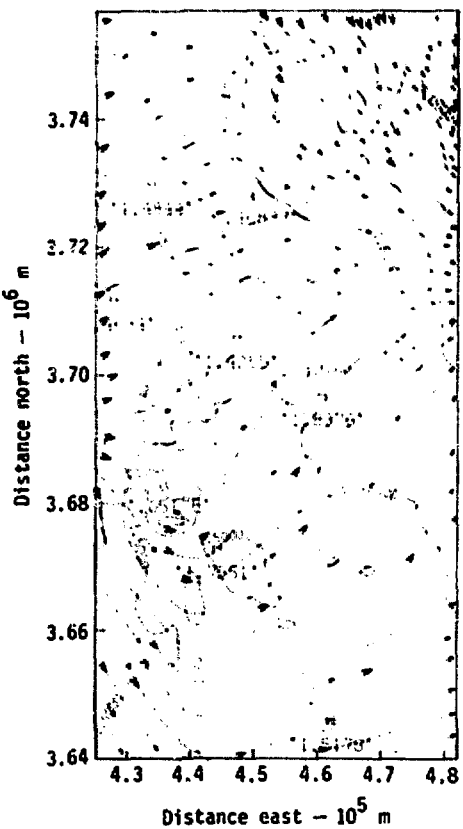

Fig. IV-8. Adjusted wind field (m/s, 60 m above the topography at 2300 EST in the Savannah River area.

pollutant plume for the Hudson River Valley at selected hours. The figures show a projection of the particle distribution on a horizontal plane. The large circle locates the assumed source. The sequence shows the effect of the wind changes (southerly to northerly and back to southerly) on the pollutant transport. Figure IV-9b at 2200 EST shows the first wind reversal toward the nighttime drainage regime as the bulk of the pollutant moved southward from the source. The trail of

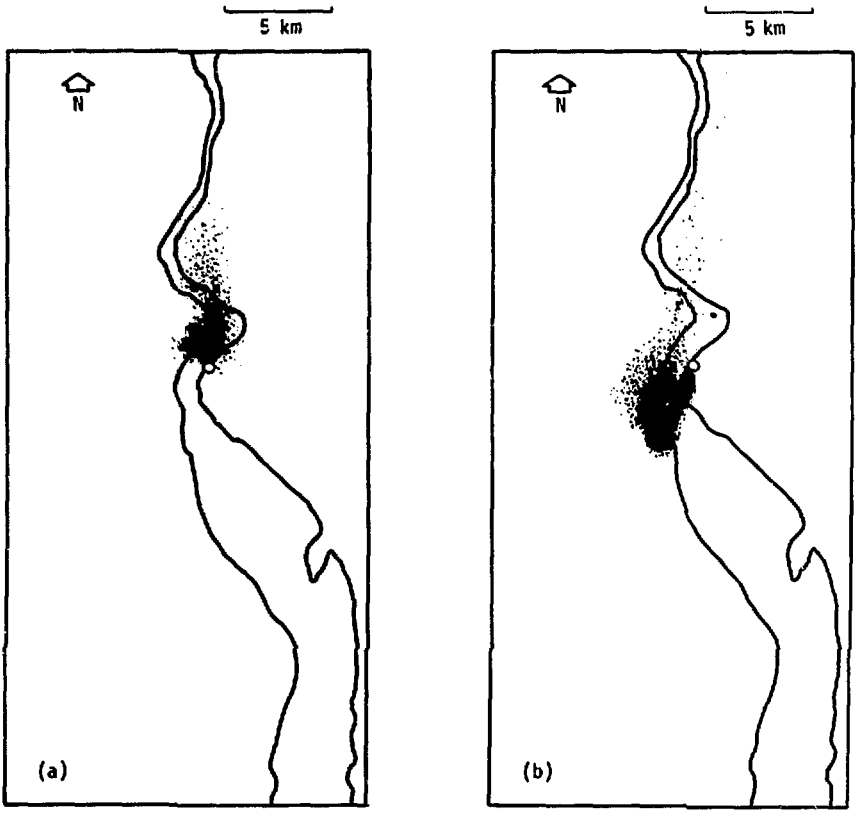

Fig. IV-9. ADPIC particle plume during the onset of the nighttime drainage regime in the Hudson River Valley: (a) 2000 EST, (b) 2200 EST.

particles north of the source indicates that at upper levels, the wind was still blowing from the south. Figure IV-11a at 0700 EST gives a good indication of the influence of topography on the plume as it meanders down the river valley and spreads out where the valley opens up toward the south. The dark lines in the particle distribution indicate topographical channeling. Figure IV-12a at 1200 EST shows the effect of the second wind reversal, establishing

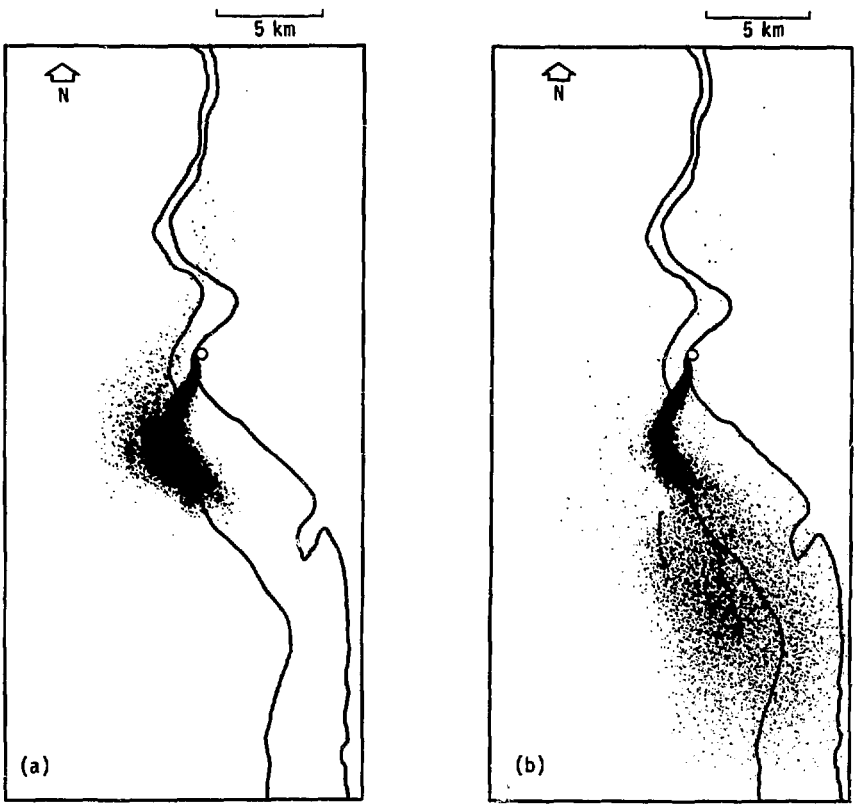

Fig. IV-10. ADPIC particle plume during the nighttime drainage regime in the Hudson River Valley: (a) 2300 EST, (b) 0100 EST.

the southerly breeze, reversing the plume, and transporting the remainder of the "old" plume back over the source region.

The output from ADPIC (discussed in the next section) is in isopleths of surface deposition and time-integrated, surface-air concentration at a height of 2 m above the topography. Surface deposition is computed in ADPIC by the usual parameterization in terms of a deposition velocity imposed on particles near the topographical

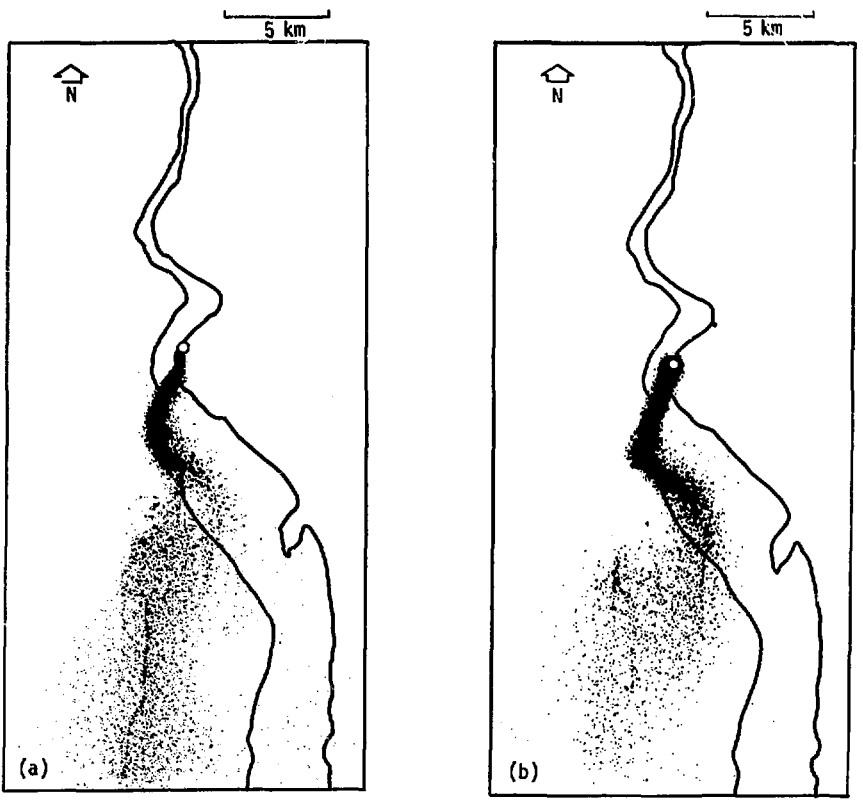

Fig. IV-11. ADPIC particle plume during the morning wind reversal in the Hudson River Valley: (a) 0700 EST, (b) 1100 EST.

boundary. For each time step, near the surface the ADPIC particles experience this deposition velocity in addition to their own diffusion and advection velocities. To obtain time-integrated, surface-air concentrations, ADPIC defines a layer of sampling volumes located at a height of 2 m above topography. During each computational cycle, the activity or mass present in each sample volume (equal to the sum of activities or masses of all the ADPIC particles present in that volume)

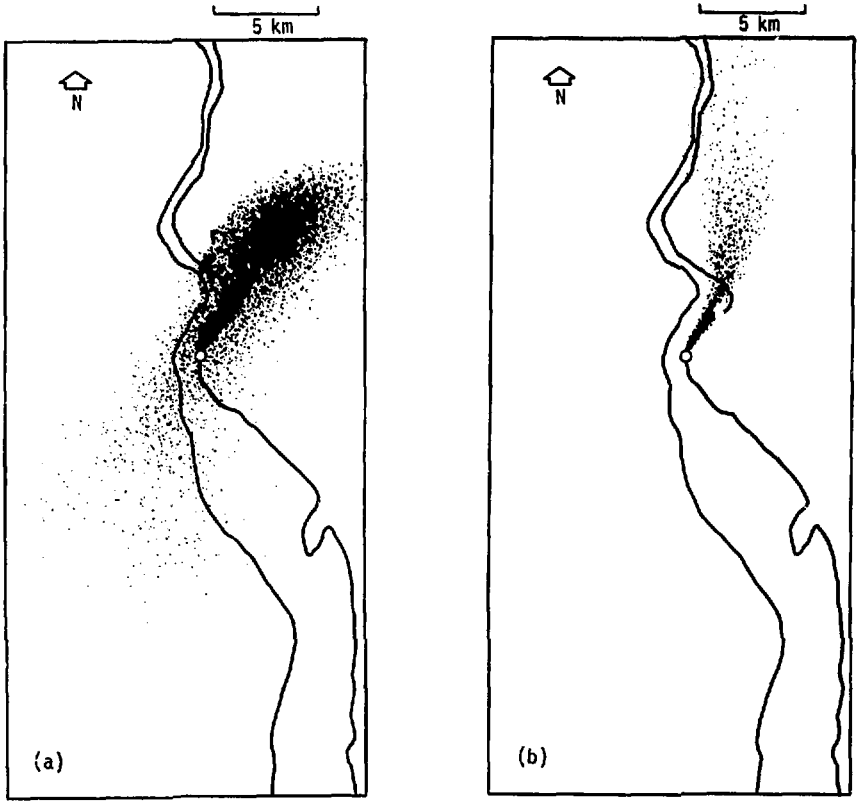

Fig. IV-12. ADPIC particle plume during the afternoon southerly breeze in the Hudson River Valley: (a) 1200 EST, (b) 1700 EST.

is multiplied by the time step and is added to the result from the previous cycle. The result is thus a time-integrated pollutant concentration over the time of the pollutant-cloud passage for each sample-volume location. The two-dimensional array of these sampling volumes stretched over the topography enables the construction of the isopleths.

V. Comparison of Results of Particle-in-Cell Model and Gaussian Model

Because of the inherent differences between a time-varying, three-dimensional model and a steady-state, unidirectional Gaussian plume model, direct comparison of concentration calculations for long distances was best obtained by isopleths overlays. For close-in comparisons (out to 5 km), we used a combination of ADPIC concentration contours overlaid with Gaussian centerline calculations and a table of the ratios of Gaussian to ADPIC calculations for 1 km increments along each Gaussian plume-centerline radial.

For the Hudson River Valley study, Figs. V-1 to V-5 show the 24-h time-integrated, surface air concentration isopleths for the four radionuclides and the inert gas. Figure V-6 shows the surface deposition velocity. The irregular contour lines are the ADPIC calculations; Gaussian results are either the sector-averaged radial arcs between the dotted lines or the oval-shaped patterns. (Except for those contours to the west, the CPS contours have been sector-averaged over 22.5°.) Isopleths for the 24-h integrated surface-air concentration are in s^2/m^3 at a height of 2 m above the topography. Isopleths for deposition are in s/m^2 and, when applicable, reflect continued radioactive decay on the ground.

The Gaussian patterns clearly show the two main meteorological regimes for the 24-h period. Isopleths toward the south-southwest result from the stable nighttime drainage wind and those to the north-northeast are from the neutral to unstable daytime breeze. In addition, there is one fan of Gaussian contours toward the west that represents the hourly average of the transition period when the wind changed direction.

The Gaussian model predicts higher concentrations along plume center lines than does the ADPIC model but these high values cover considerably less area. We expected to find this trend because the Gaussian model integrates a set of

Figs. V-1 to V-6. Isopleths of 24-h, time-integrated, relative surface-air concentration in s^2/m^3 (Figs. V-1 to V-5) and ground deposition in s/m^2 (Fig. V-6) for the Hudson River Valley. Irregular contour lines are ADPIC concentrations; uniform contour lines are nonsector-averaged Gaussian concentrations; solid arcs are sector-averaged Gaussian concentrations within the 22.5° sectors (dotted lines). Enlargements of these contours out to 5 km from the source are shown in Figs. V-7 to V-12.

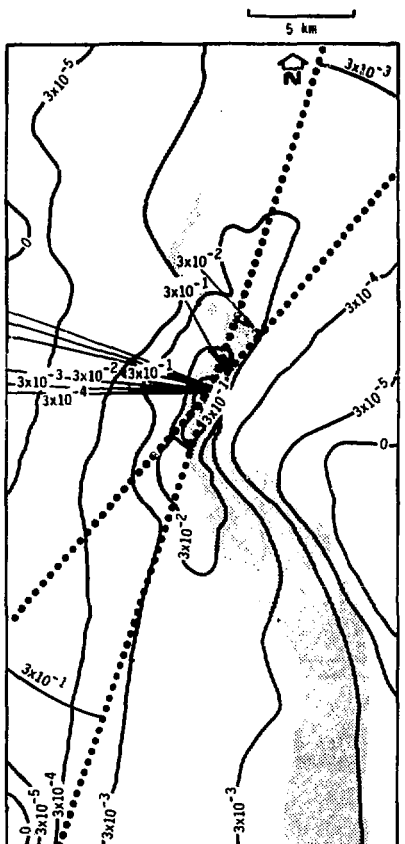

Fig. V-1. Relative surface-air concentration isopleths for inert gas.

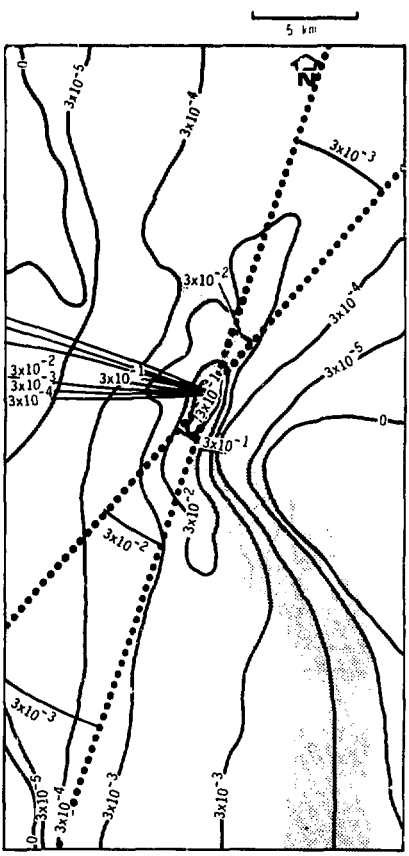

Fig. V-2. Relative surface-air concentration isopleths for ^{131}I.

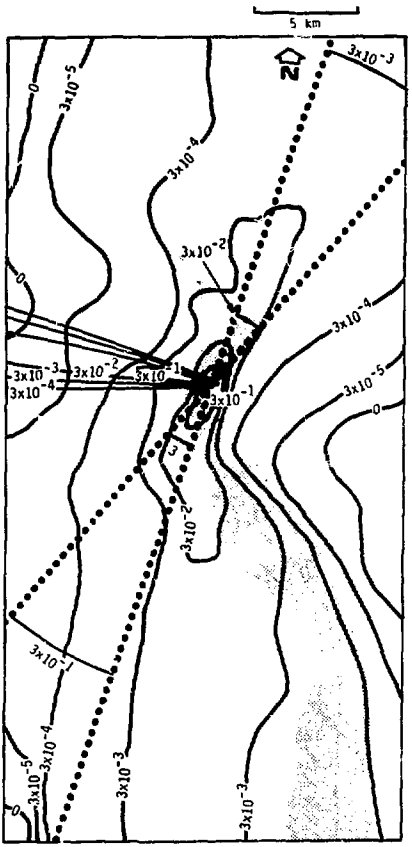

Fig. V-3. Relative surface-air concentration isopleths for ^{133m}Xe.

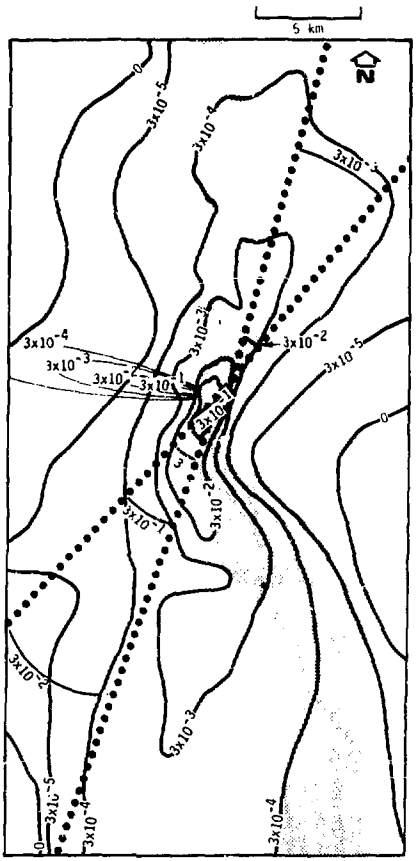

Fig. V-4. Relative surface-air concentration isopleths for ^{88}Kr.

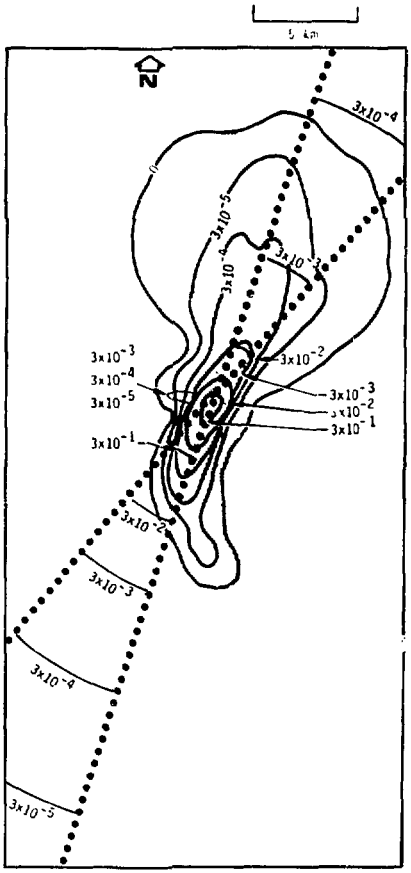

Fig. V-5. Relative surface-air concentration isopleths for ^{138}Xe.

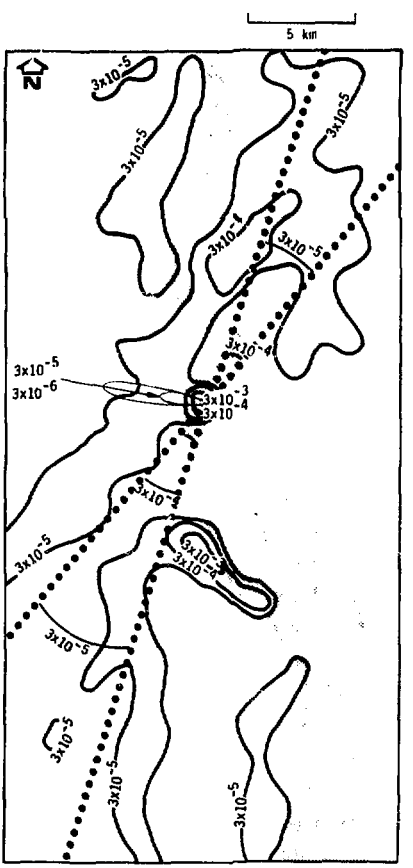

Fig. V-6. Relative ground deposition isopleths for ^{131}I.

stationary plumes of infinite extent, thus calculating a contribution in areas where the pollutant never reached. An example of this is the westerly plume resulting from the period of wind shift from northerly to southerly. ADPIC contours in this direction indicate concentrations of several orders of magnitude less. The high cliffs on the east bank of the river and the transitory nature of the wind prevented the bulk of the pollutant from reaching the distances indicated by the Gaussian model during the wind shift period. Also, the presence of surface air pollutants over a much larger area as shown by the ADPIC contours is the result of exposure from the returning diffuse, secondary pollutant caused by the shifting and reversals of the wind during the 24-h period. This feature is not considered by the Gaussian model.

The greatest difference between the two models manifests itself under the stable nighttime drainage regime that gives rise to the south-southwesterly plume contours. Here, the Gaussian model exhibits integrated centerline concentrations much higher than those of ADPIC. The Gaussian formula predicts infinite concentrations as the mean wind $\bar{u}$ goes to zero. For stable conditions in this study, the mean wind near the surface was $\bar{u} < 0.5$ m/s, a value that is very close to the singularity in the equation. Consequently, high concentrations were calculated by the Gaussian model. In addition, recent experiments by Sagendorf and Dickson[15] indicate that, under low wind speed inversion conditions similar to those prevailing here, the wind is often variable as near-calm is approached and the standard sector averaging method for the Gaussian model may be conservative. This contention is supported by Yanskey and Markee.[16] The Markee curves for an F category nearly correspond to those of a typical Pasquill B for which the standard deviation of the horizontal wind direction fluctuation, $\sigma_H \simeq 20°$.

An equally important difference between the models arises from the influence exerted on them by the topography. The ADPIC contours clearly exhibit the channeling effect of the river valley on the wind but the simple Gaussian model, because it is based on the local mean wind at the source only, cannot account for this effect. This again is illustrated by the direction of the south-southwest nighttime Gaussian plume.

Figures V-1 to V-5 are arranged to show all the comparison plots (out to 70 km from the source) for

the five species in order of decreasing half-life and consequently, they show ever decreasing contour areas. The above discussion applies to all these figures. Figure V-6 presents the deposition isopleths for ^{131}I, the only species that had a deposition velocity of 0.005 m/s. Once again, the preceding discussion applies with the additional observation that most of the material is deposited near the source as might be expected for a surface release. The only other region of high deposition is a ridge on the east bank of the river, south of the source.

Figures V-7 to V-12 show a magnified area of ADPIC contours (out to 5 km from the source) corresponding to the full scale Figs. V-1 to V-6. The Gaussian plume centerlines are shown and the hashmarks along these centerlines are at 1 km intervals. For each of these intervals, the ratios of the ADPIC contour values to the time-integrated concentrations at the Gaussian plume centerlines are listed in Tables V-1 to V-6.

This magnified comparison of the two assessment models reveals the same features as seen by the regional comparison. Because of the cell averaging involved (0.5 km cells in this case), the concentrations calculated by ADPIC for distances less than 1 km from the source must be expected to be too low. For a comparison at such distances, ADPIC would have to be run with a finer grid mesh. When evaluating the close-in comparisons, it is important to observe that the Gaussian model concentrates the total pollutant for the 24 h in discrete plumes while the ADPIC model spreads the pollutant over the entire area, corresponding to the time variability of the winds. This explains why the Gaussian centerline concentrations are always higher than the ADPIC contour values.

One point remains to be mentioned in regard to the MATHEW-ADPIC treatment of the boundary condition at the topography. If a strict fluid dynamical boundary condition of the wall is invoked, *all* velocities should go to zero at the topography. This presents a difficulty when ADPIC particles diffuse to within an infinitesimal distance of the boundary. At such a point, if the pollutant does *not* deposit (e.g., all but the ^{131}I), the particles will essentially come to rest. As a result, if an integrated surface air concentration is calculated, these particles contribute *ad infinitum*, a condition that clearly is not physically correct. For this reason, the topographical boundary condition in MATHEW is taken to be the velocity of the mean wind at the roughness

Table V-1. Ratio of Gaussian to ADPIC time-integrated concentration values for inert gas from Fig. V-7 as a function of the distance along Gaussian plume centerlines.

Distance	Plume centerline		
km	I	II[a]	III[a]
1	58	2.5	7.5
2	162	1.5	21
3	270	1.7	26
4	900	2.4	31
5	2700	1.7	110

[a]Gaussian values are sector-averaged.

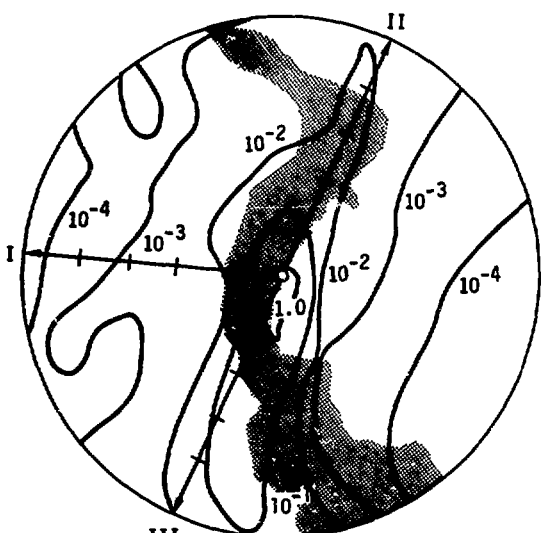

Fig. V-7. Isopleths of 24-h, time-integrated, relative surface-air concentration (s^2/m^3) for inert gas out to 5 km from the Hudson River Valley source. Radial tickmarks are at 1-km intervals along the numbered Gaussian plume centerlines.

Table V-2. Ratio of Gaussian to ADPIC time-integrated concentration values for ^{131}I from Fig. V-8 as a function of the distance along Gaussian plume centerlines.

Distance	Plume centerline		
km	I	II[a]	III[a]
1	19	2.1	3.2
2	11	1.2	2.6
3	15	2.7	1.3
4	33	2.8	2.7
5	47	4.0	5.8

[a]Gaussian values are sector-averaged.

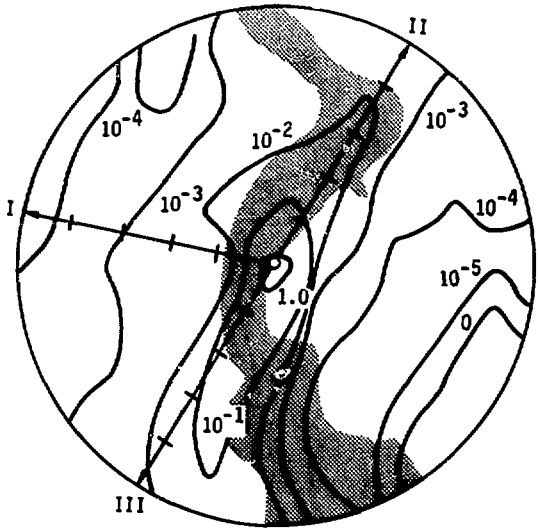

Fig. V-8. Isopleths of 24-h, time-integrated, relative surface-air concentration (s^2/m^3) for ^{133}I out to 5 km from the Hudson River Valley source. Radial tickmarks are at 1-km intervals along the numbered Gaussian plume centerlines.

Table V-3. Ratio of Gaussian to ADPIC time-integrated concentration values for ^{133m}Xe from Fig. V-9 as a function of the distance along Gaussian plume centerlines.

Distance	Plume centerline		
km	I	II[a]	III[a]
1	58	2.5	9.2
2	150	1.5	20
3	250	1.8	25
4	660	2.4	60
5	2400	2.1	140

[a]Gaussian values are sector-averaged.

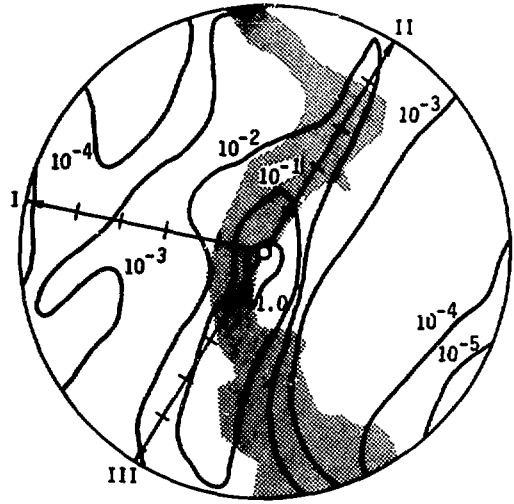

Fig. V-9. Isopleths of 24-h, time-integrated, relative surface-air concentrations (s^2/m^3) for ^{133m}Xe out to 5 km from the Hudson River Valley source. Radial tickmarks are at 1-km intervals along the numbered Gaussian plume centerlines.

Table V-4. Ratio of Gaussian to ADPIC time-integrated concentration values for ^{88}Kr from Fig. V-10 as a function of the distance along Gaussian plume centerlines.

Distance	Plume centerline		
km	I	II[a]	III[a]
1	160	2.3	8.3
2	190	1.4	23
3	180	1.6	15
4	870	2.0	36
5	2900	2.0	160

[a]Gaussian values are sector-averaged.

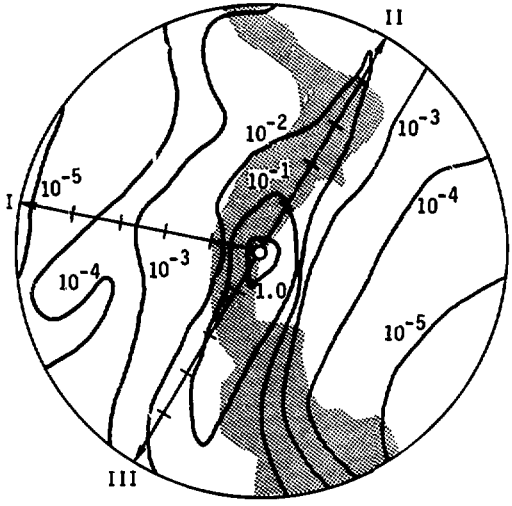

Fig. V-10. Isopleths of 24-h, time-integrated, realtive surface-air concentration (s^2/m^3) for ^{88}Kr out to 5 km from the Hudson River Valley source. Radial tickmarks are at 1-km intervals along the numbered Gaussian plume centerlines.

Table V-5. Ratio of Gaussian to ADPIC time-integrated concentration values for ^{138}Xe from Fig. V-11 as a function of the distance along Gaussian plume centerlines.

Distance	Plume centerline		
km	I	II[a]	III[a]
1	2600	5.0	12
2	1500	6.4	17
3	∞	3.8	24
4	∞	5.5	110
5	∞	6.2	5200

[a]Gaussian values are sector-averaged.

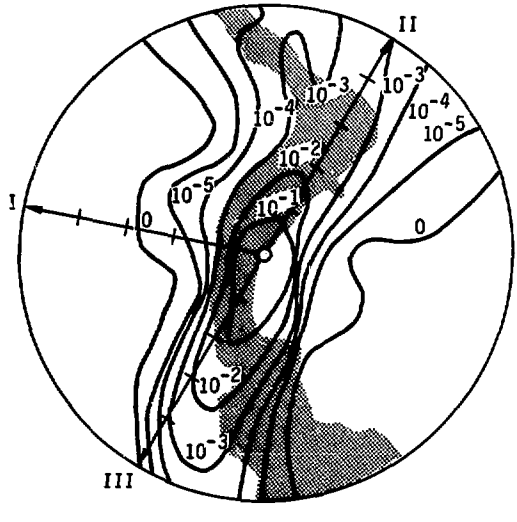

Fig. V-11. Isopleths of 24-h, time-integrated, relative surface-air concentration (s^2/m^3) for ^{138}Xe out to 5 km from the Hudson River Valley source. Radial tickmarks are at 1-km intervals along the numbered Gaussian plume centerlines.

Table V-6. Ratio of Gaussian to ADPIC surface deposition values for ^{131}I from Fig. V-12 as a function of the distance along Gaussian plume centerlines.

Distance	Plume centerline		
km	I	II[a]	III[a]
1	1.7	›	300
2	1.0	∞	∞
3	1.0	∞	130
4	1.7	∞	∞
5	2.1	∞	250

[a]Gaussian values are sector-averaged.

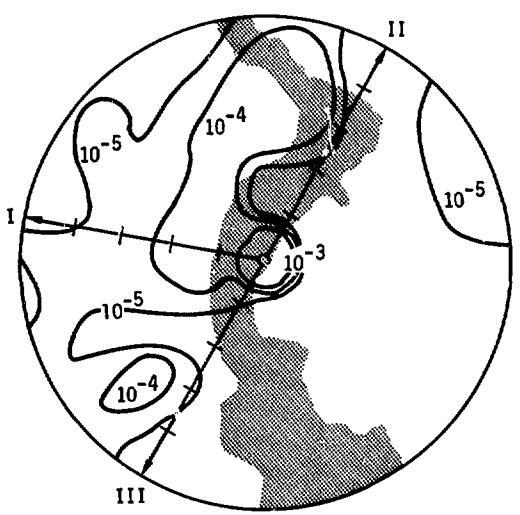

Fig. V-12. Isopleths of 24-h, time-integrated, relative ground deposition (s/m^2) for ^{131}I out to 5 km from the Hudson River Valley source. Radial tickmarks are at 1-km intervals along the numbered Gaussian plume centerlines.

height z_o. In this way, a slip velocity is created that will prevent ADPIC particles from stagnating at heights $z < z_o$. For strongly varying topography (e.g., cliffs) as in the Hudson River Valley, this can result in the local impaction of particles onto the topography. Such impaction is depicted in Fig. V-13 for the inert gas species. Whether this impaction model has merit for neutrally buoyant, inert contaminants is not yet clear. However, it is an attempt to parameterize the physical processes at heights less than z_o. In any event, the effects of impaction are small compared to the other results of this study.

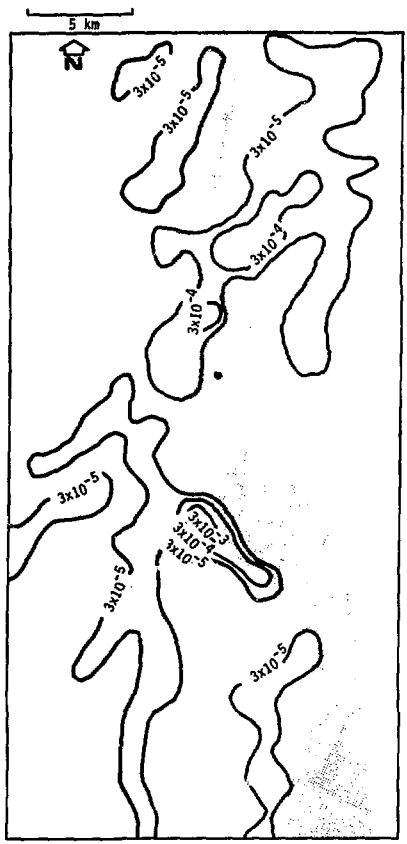

Fig. V-13. Hudson River Valley 24-h relative surface impaction (s/m^2) for inert gas.

Figures V-14 to V-26 and Tables V-7 to V-12 show a parallel sequence of results for the southeastern U.S. site. The discussion comparing the ADPIC model to the Gaussian formula for the Hudson River Study applies. The most salient point in this case is the contribution of the secondary (returning) pollutant. During the early morning hours at this site, the wind is very light and slowly varying, which generates an extended, diffuse secondary pollutant source. The following day, this wind regime transports the extended source toward the north-northeast. ADPIC contour values of time-integrated, surface-air concentrations cover a much larger area in that direction than do those of the Gaussian model because the Gaussian code uses sector-averaging in this direction only. This feature can be seen

Figs. V-14 to V-19. Isopleths of 24-h, time-integrated, relative surface-air concentration in s^2/m^3 (Figs. V-14 to V-18) and ground deposition in s/m^2 (Fig. V-19) for the southeastern U.S. site. Irregular contour lines are ADPIC concentrations; uniform contour lines are nonsector-averaged Gaussian concentrations; solid arcs are sector-averaged Gaussian concentrations within the 22.5° sectors (dotted lines). Enlargements of these contours out to 5 km from the source are shown in Figs. V-21 to V-26.

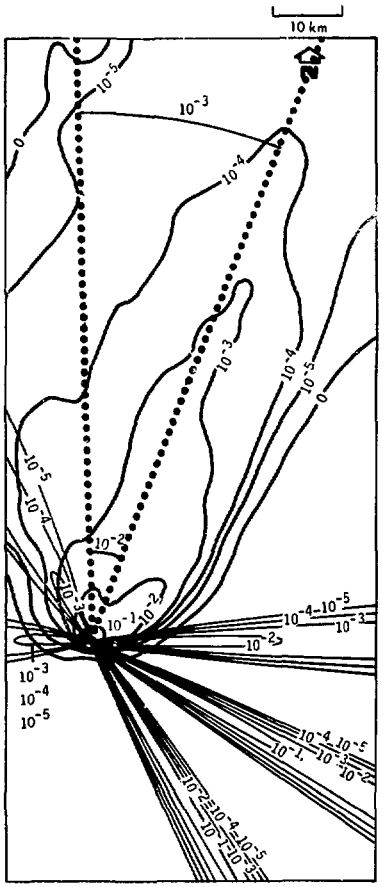

Fig. V-14. Relative surface-air concentration isopleths for inert gas.

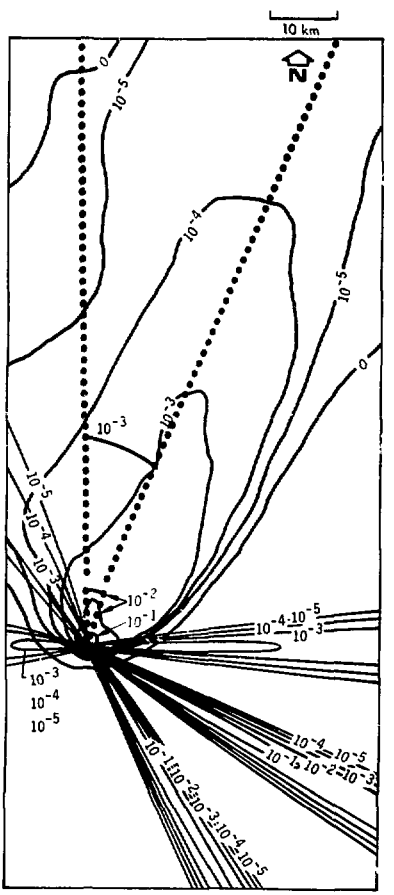

Fig. V-15. Relative surface-air concentration isopleths for ^{131}I.

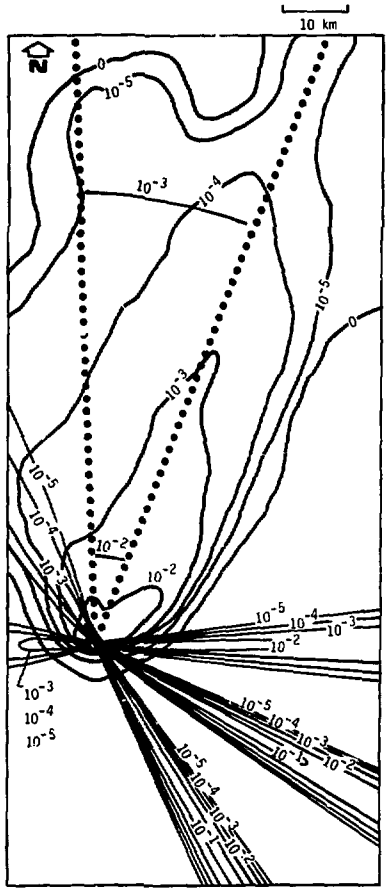

Fig. V-16. Relative surface-air concentration isopleths for ^{133m}Xe.

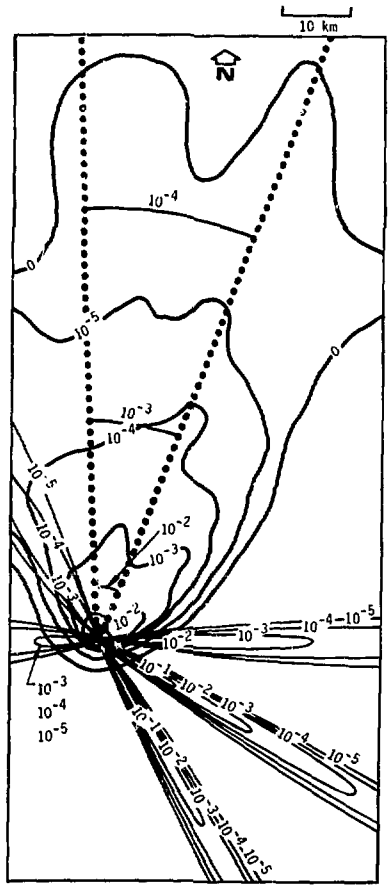

Fig. V-17. Relative surface-air concentration isopleths for ^{88}Kr.

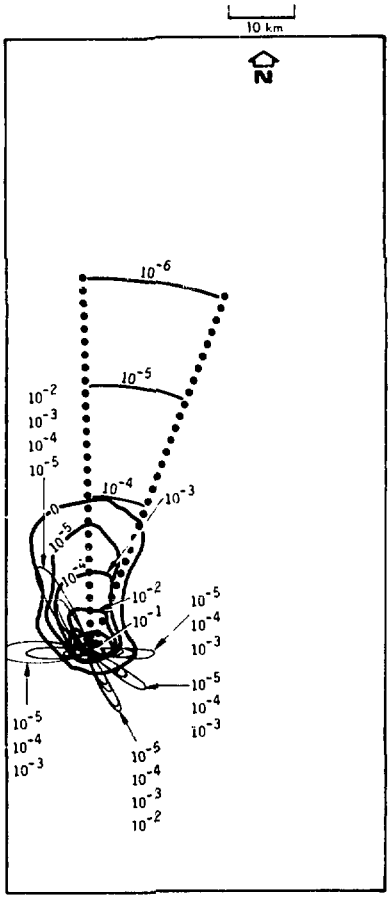

Fig. V-18. Relative surface-air concentration isopleths for ^{138}Xe.

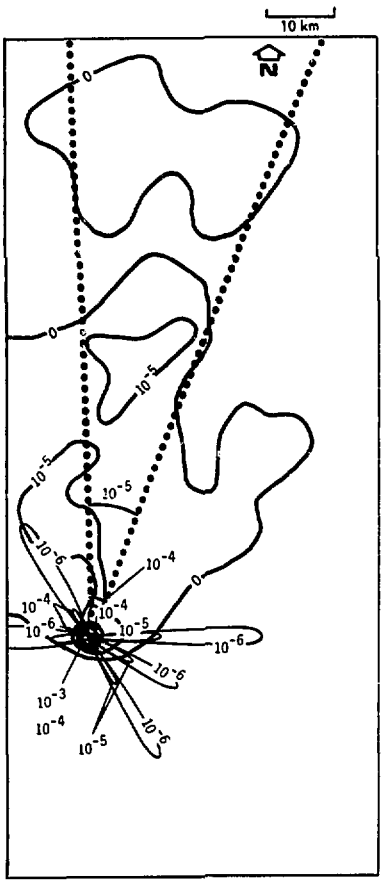

Fig. V-19. Relative ground deposition isopleths for ^{131}I.

Fig. V-20. Southeastern U.S. 24-h, relative surface impaction (s/m^2) for inert gas.

by comparing the results shown in Figs. V-14 to V-18. Thus, even the sector-averaged Gaussian plume in this direction covers less area and shows higher concentrations than do the ADPIC contours.

Another reason for the higher Gaussian model values along the plume centerlines is that this model can only use the wind direction at the source whereas the MATHEW code generates a regional wind field that, at greater distances, may differ in direction from the wind field at the source. This causes the misalignment of the Gaussian sector-averaged plume in the north-northeast direction with respect to the ADPIC contours and appears in Figs. V-14 to V-19. Figures V-21 to V-26 and Tables V-7 to V-12 show the resulting large ratios of Gaussian to ADPIC concentrations.

In these two studies, the grid was initially free from any pollutant with no background present from previous hours. To determine the effect of this initial condition, the Hudson River Valley study was run for an additional 24-h meteorological cycle, identical to the first one; no Gaussian calculations were conducted Figures V-27 to V-33 depict the results of the 48-h time-integrated surface air concentrations and the 48-h ground deposition. This set of figures corresponds directly to the 24-h set for this site discussed earlier in Figs. V-1 to V-7.

As expected, all concentrations are higher although the expected

factor-of-two difference for the time-integrated, surface-air dose is difficult to discern because the contour levels are an order of magnitude apart. The effect of the empty grid initial condition is also very difficult to separate out on these plots. Therefore to obtain a quantitative estimate of this effect, the total amount of pollutant present in the ADPIC grid at each hour during the first 24-h cycle was compared with the amount present at corresponding hours from the second 24-h run or 1 d later (see Fig. V-34). The absolute value of ΔQ, the difference between the pollutant present at hour i and hour i + 24 h, divided by the average amount present $\bar{Q}$ is plotted against the hour i:

$$\left|\frac{\Delta Q}{\bar{Q}}\right| = \frac{Q_{i+24} - Q_i}{(Q_{i+24} + Q_i)/2} .$$

The effect of the empty grid initial condition becomes negligible after 6 h into the second 24-h run. The remaining 1% difference is a measure of the statistical accuracy of the ADPIC code in duplicating identical problems.*

*ADPIC is *not* a statistical transport code, although the initial coordinates for the many thousands of particles needed to model the source term distribution are picked randomly, subject to a Gaussian distribution.

Table V-7. Ratio of Gaussian to ADPIC time-integrated concentration values for inert gas from Fig. V-21 as a function of the distance along Gaussian plume centerlines.

Distance	Plume centerline					
km	I	II	III[a]	IV	V	VI
1	3.1	3.2	8.1	3.2	26	72
2	18	2.2	8.0	2.9	15	72
3	89	1.4	8.3	2.0	20	1400
4	96	1.1	2.8	4.0	38	∞
5	78	0.9	8.8	120	∞	∞

[a]Gaussian values are sector-averaged.

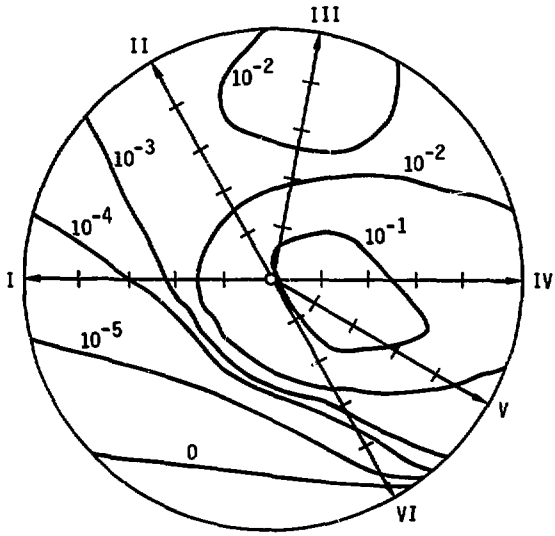

Fig. V-21. Isopleths of 24-h, time-integrated, relative surface-air concentration (s^2/m^3) for inert gas out to 5 km from the southeastern U.S. source. Radial tickmarks are at 1-km intervals along the numbered Gaussian plume centerlines.

Table V-8. Ratio of Gaussian to ADPIC time-integrated concentration values for ^{131}I from Fig. V-22 as a function of the distance along Gaussian plume centerlines.

Distance	Plume centerline					
km	I	II	III[a]	IV	V	VI
1	2.7	2.8	12	3.9	12	21
2	16	2.0	10	3.2	13	30
3	40	1.1	6.0	3.4	11	320
4	72	0.8	1.5	4.4	13	2000
5	170	1.1	1.1	3.3	83	∞

[a]Gaussian values are sector-averaged.

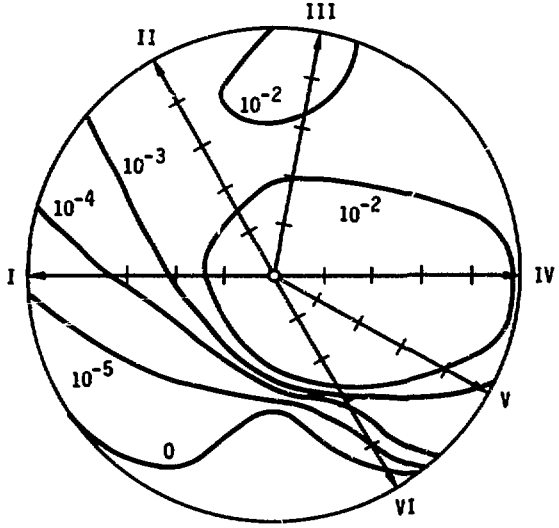

Fig. V-22. Isopleths of 24-h, time-integrated, relative surface-air concentration (s^2/m^3) for ^{131}I out to 5 km from the southeastern U.S. source. Radial tickmarks are at 1-km intervals along the numbered Gaussian plume centerlines.

Table V-9. Ratios of Gaussian to ADPIC time-integrated concentration values for ^{133m}Xe from Fig. V-23 as a function of the distance along Gaussian plume centerlines.

Distance	Plume centerline					
km	I	II	III[a]	IV	V	VI
1	3.0	3.2	8.1	3.0	26	72
2	9.0	2.2	8.0	2.8	15	140
3	14	1.5	8.0	2.1	22	2800
4	29	1.2	2.7	4.0	75	∞
5	47	1.2	2.0	8.6	160	∞

[a]Gaussian values are sector-averaged.

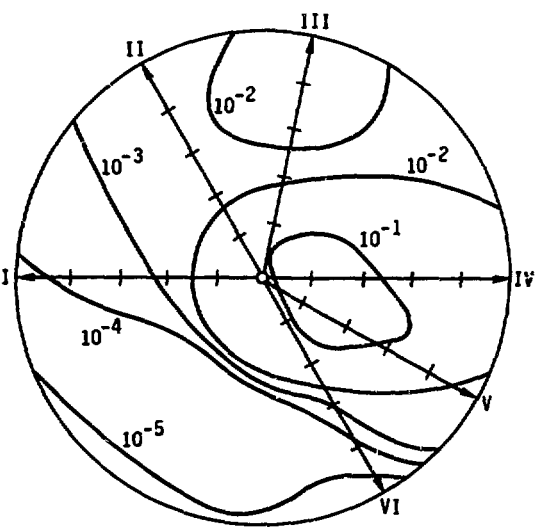

Fig. V-23. Isopleths of 24-h, time-integrated, relative surface-air concentration (s^2/m^2) for ^{133m}Xe out to 5 km from the southeastern U.S. source. Radial tickmarks are at 1-km intervals along the numbered Gaussian plume centerlines.

Table V-10. Ratios of Gaussian to ADPIC time-integrated concentration values for ^{88}Kr from Fig. V-24 as a function of the distance along Gaussian plume centerlines.

Distance	Plume centerline					
km	I	II	III[a]	IV	V	VI
1	3.0	3.1	7.8	5.6	46	72
2	17	2.1	7.5	2.5	25	120
3	91	1.3	10	1.8	21	2100
4	260	1.0	4.4	2.9	49	∞
5	340	1.6	4.4	6.0	110	∞

[a]Gaussian values are sector-averaged.

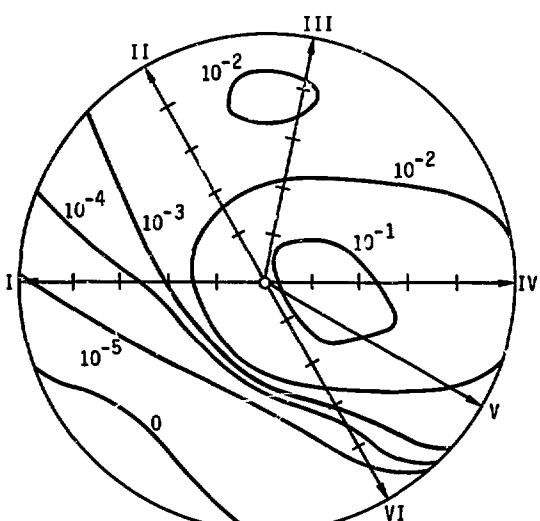

Fig. V-24. Isopleths of 24-h, time-integrated, relative surface-air concentration (s^2/m^3) for ^{88}Kr out to 5 km from the southeastern U.S. source. Radial tickmarks are at 1-km intervals along the numbered Gaussian plume centerlines.

Table V-11. Ratios of Gaussian to ADPIC time-integrated concentration values for ^{138}Xe from Fig. V-25 as a function of the distance along Gaussian plume cemter;omes/

Distance	Plume centerline					
km	I	II	III[a]	IV	V	VI
1	5.3	5.5	12	11	75	210
2	14	7.0	9.9	7.0	55	160
3	290	5.8	12	5.7	43	6500
4	850	3.3	10	9.3	67	∞
5	∞	1.9	11	15	150	∞

[a]Gaussian values are sector-averaged.

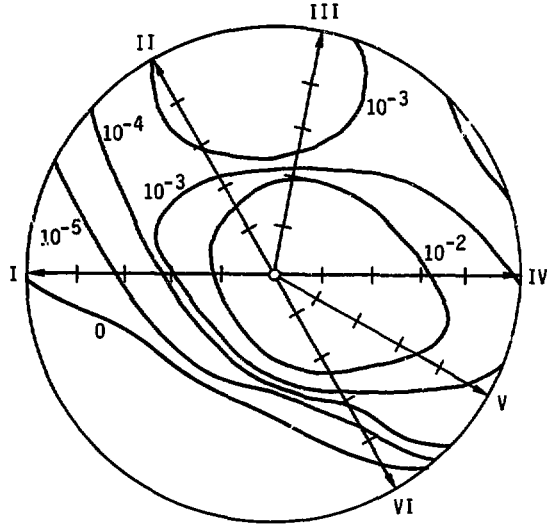

Fig. V-25. Isopleths of 24-h, time-integrated, relative surface-air concentration (s^2/m^3) for ^{138}Xe out to 5 km from the southeastern U.S. source. Radial tickmarks are at 1-km intervals along the numbered Gaussian plume centerlines.

Table V-12. Ratio of Gaussian to ADPIC surface deposition values for ^{131}I from Fig. V-26 as a function of distance along Gaussian plume centerline.

Distance	Plume centerline					
km	I	II	III[a]	IV	V	VI
1	1.3	1.4	8.5	1.4	4.2	7.8
2	4.0	7.9	6.1	1.2	3.1	14
3	4.8	13	11	4.0	98	19
4	15	6.0	17	5.0	75	∞
5	∞	2.3	25	7.0	56	∞

[a]Gaussian values are sector-averaged.

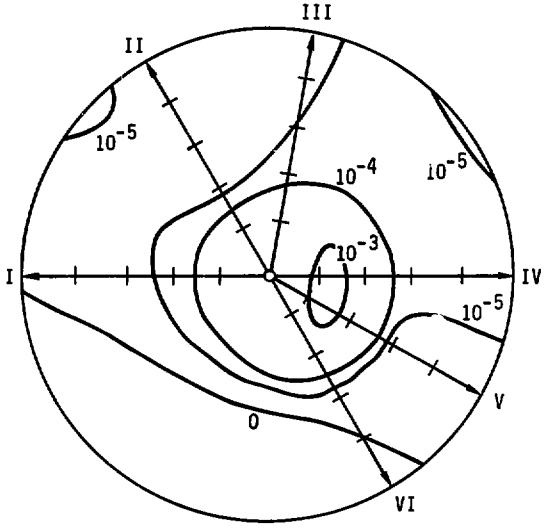

Fig. V-26. Isopleths of 24-h, time-integrated, relative ground deposition (s/m^2) for ^{131}I out to 5 km from the southeastern U.S. source. Radial tickmarks are at 1-km intervals along the numbered Gaussian plume centerlines.

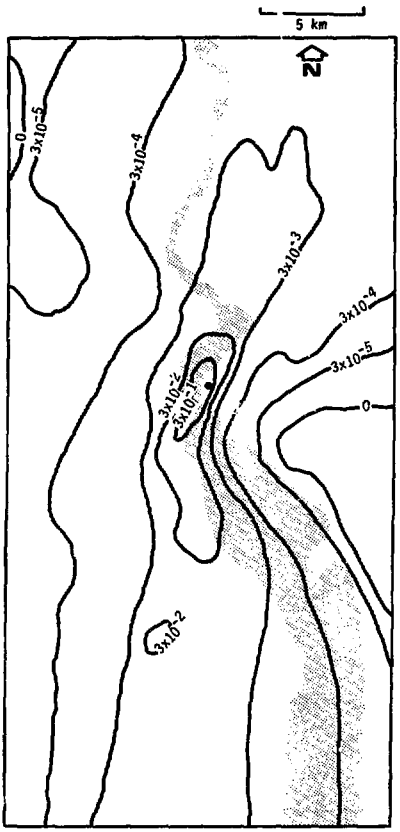

Fig. V-27. Hudson River Valley 48-h, time-integrated, relative surface-air concentrations (s^2/m^3) for inert gas.

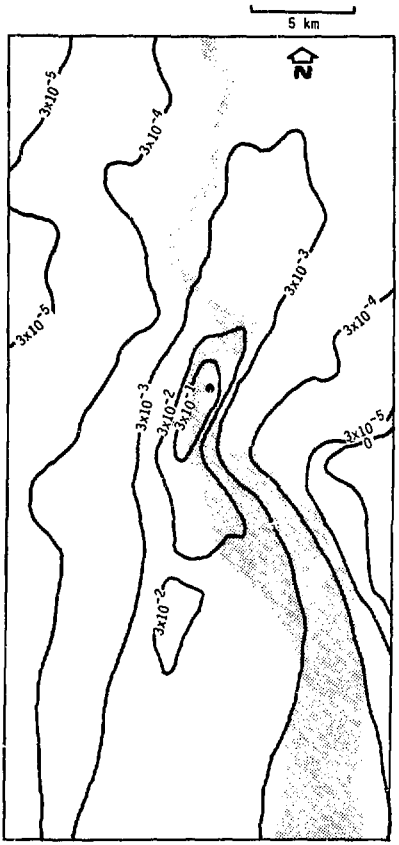

Fig. V-28. Hudson River Valley 48-h, time-integrated, relative surface-air concentrations (s^2/m^3) for ^{131}I.

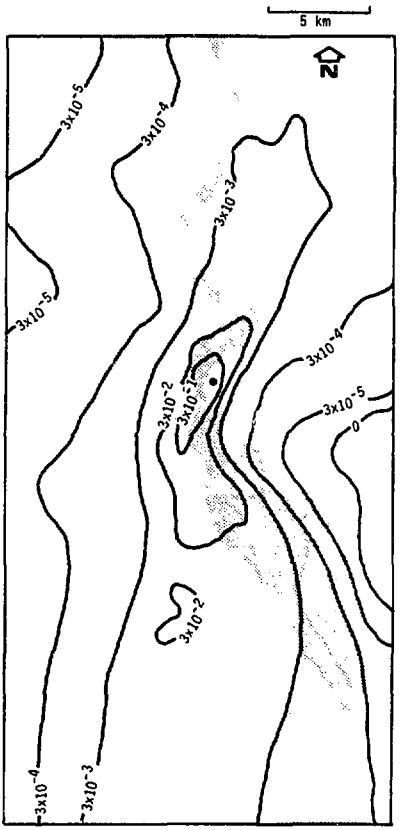

Fig. V-29. Hudson River Valley 48-h, time-integrated, relative surface-air concentrations (s^2/m^3) for ^{131m}Xe.

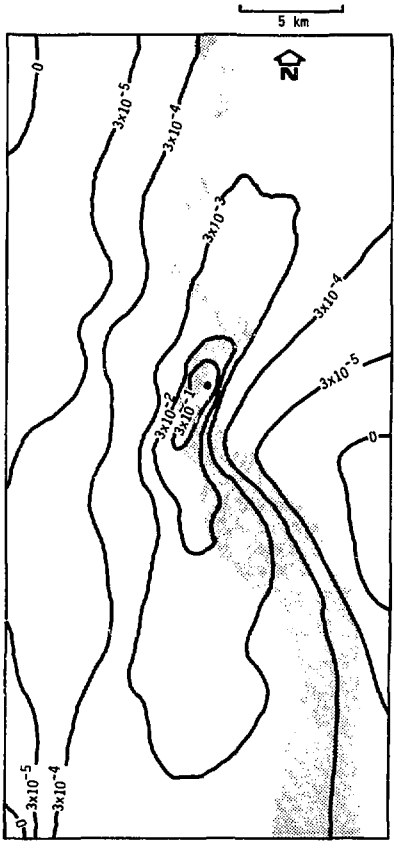

Fig. V-30. Hudson River Valley 48-h, time-integrated, relative surface-air concentrations (s^2/m^3) for ^{88}Kr.

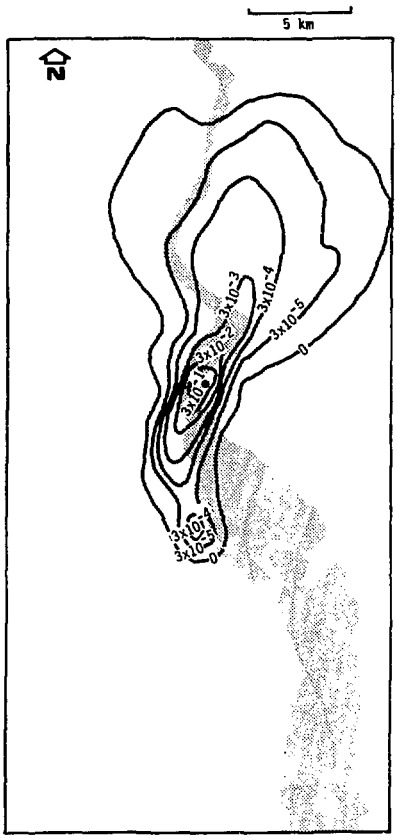

Fig. V-31. Hudson River Valley 48-h, time-integrated, relative surface-air concentrations (s^2/m^3) for ^{138}Xe.

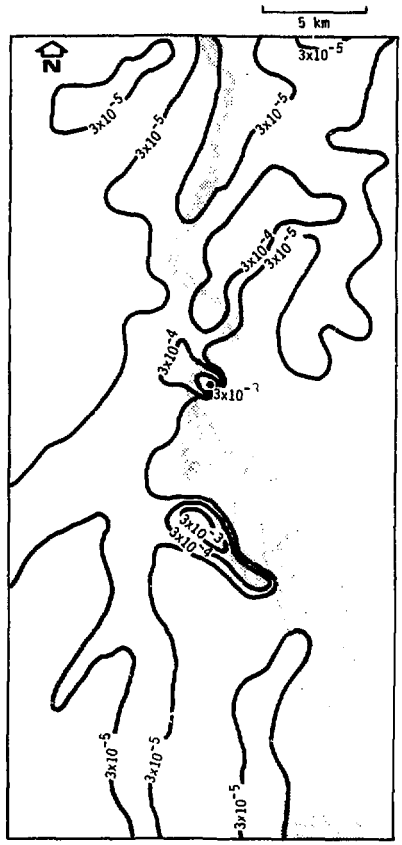

Fig. V-32. Hudson River Valley 48-h, relative surface deposition (s/m^2) for ^{131}I.

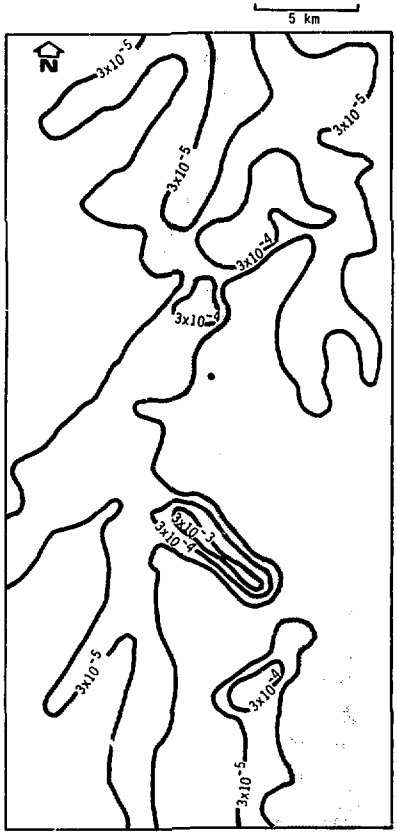

Fig. V-33. Hudson River Valley 48-h, relative surface impaction (s/m^2) for inert gas.

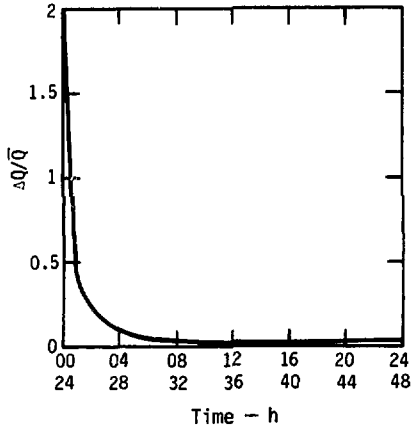

Fig. V-34. Relative difference of total pollutant ($\Delta Q/\bar{Q}$) in the ADPIC grid at corresponding hours, one day apart for the Hudson River Valley.

VI. Conclusions and Recommendations

Three-dimensional, time-dependent PIC model calculations exhibit several advantages over steady state Gaussian models for assessment calculations. PIC models more closely simulate the three-dimensional physical processes of the planetary boundary layer. This appears clearly when sites with strong individual topographic and meteorological features are considered. The Hudson River Valley is an area in which the local topography strongly influences the day and nighttime meteorological regimes. Under these circumstances, the results of the PIC and Straight-Line Airflow Gaussian methods differed greatly. Overall, the Gaussian method calculated higher concentrations under stable conditions; agreement between the two methods was better for neutral to unstable conditions. The PIC method calculated air concentrations over larger areas than did the Gaussian model, because of its inclusion of meandering and secondary exposure from the returning plume after flow reversal.

These differences are less evident for the southeastern U.S. site where the topography does not play as major a role. However, at the southeastern U.S. site, when the light nighttime winds are followed by a steady flow during the day, there are again large differences between the two methods as the Gaussian model overestimates integrated air concentrations and ground deposition.

For this study, the 24-h runs were sufficient to draw a comparison between the two methods for estimating air concentration and deposition. However, a follow-up study is indicated to determine if these differences persist for longer periods of time. We recommend that techniques be developed so that at the least, yearly assessments can be calculated economically with the PIC method.

Acknowledgment

This work was performed under the auspices of the U.S. Energy Research & Development Administration, under contract No. W-7405-Eng-48 and was sponsored by the Nuclear Regulatory Commission (NRC), under Work Authorization A0158.

References

1. *Methods for Estimating Atmospheric Transport and Dispersion of Gaseous Effluents in Routine Releases from Light-Water-Cooled Reactors* (U.S. Nuclear Regulatory Commission, Washington, D.C., 1976), Regulatory Guide 1.111.
2. J.I. Van der Hoven, C.R. Dickson, C.E. Start, and L.L. Wendell, "Recent Analytical and Experimental Efforts on Single-Source Effluent Dispersion to Distances of 100 km," in *Proc. of Joint Symposium of the International Atomic Energy Agency and the World Meteorological Organization*, (Vienna, 1974) IAEA-SM-181/8.
3. K.R. Peterson, T.V. Crawford, and L.A. Lawson, "CPS: A Continuous Point Source Computer Code for Plume Dispersion and Deposition Calculations," Lawrence Livermore Laboratory, Rept. UCRL-52049 (1976).
4. J. F. Sagendorf, "A Program for Evaluating Atmospheric Dispersion from a Nuclear Power Station," National Ocean and Atmospheric Administration, Air Resources Laboratory, Idaho Falls, Idaho, Technical Memorandum ERL-42 (1974).
5. D. H. Slade, "Meteorology and Atomic Energy," Energy Research and Development Administration, Rept. TID-24190 (1968).
6. C.A. Sherman, "A Mass-Consistent Model for Wind Fields Over Complex Terrain," Lawrence Livermore Laboratory, Rept. UCRL-76161 Rev. 1 (1975). Submitted to the *Journal of Applied Meteorology*.
7. C.A. Sherman, "MATHEW: A Mass-Consistent Wind Field Model," Ph.D. thesis, University of California, Davis, CA, to be published.
8. R. Lange, "ADPIC — A Three-Dimensional Computer Code for the Study of Pollutant Dispersal and Deposition Under Complex Conditions," Lawrence Livermore Laboratory Rept. UCRL-51462 (1973).
9. R. Lange, and J.B. Knox, "Adaption of a Three-Dimensional Atmospheric Transport and Diffusion Model to Rainout Assessments," Lawrence Livermore Laboratory, Rept. UCRL-75731 (1974).
10. P.H. Gudiksen, K.R. Peterson, R. Lange, and J.B. Knox, "Plume Depletion Following Postulated Plutonium Dioxide Releases from Mixed-Oxide Fuel-Fabrication Plants," Lawrence Livermore Laboratory, Rept. UCRL-51781 (1975).

11. R. Lange, "ADPIC — A Three-Dimensional Transport-Diffusion Model for the Dispersal of Atmospheric Pollutants and Its Validation Against Regional Tracer Studies," Lawrence Livermore Laboratory, Rept. UCRL-76170, Rev. 1 (1975). Submitted to the *Journal of Applied Meteorology*.

12. M.H. Dickerson, and R.C. Orphan, "Atmospheric Release Advisory Capability," *Nuclear Safety, 17* (3), p. 281 (1976).

13. "Preliminary Safety Analysis Report for Indian Point Nuclear Generating Unit No. 3," Con-Edison Company of New York (1973).

14. T.M. Langley, and W.L. Martin, "The Savannah River Plant Site," E.I. du Pont de Nemours and Company, Rept. DP1323 (1973).

15. J.F. Sagendorf, and C.R. Dickson, "Diffusion Under Low Wind Speed, Inversion Conditions," National Oceanic and Atmospheric Administration Technical Memorandum ERL ARL-52 (1974).

16. G.R. Yanskey, E.H. Markee, Jr., and A.P. Richter, "Climatology of the National Reactor Testing Station," U.S. Atomic Energy Commission, Idaho Falls, Idaho, Rept. IDO-12048 (1966).

PLL/gw/vt/gw

Appendix A: Comparison of ADPIC and Gaussian Plume Depletion Factors

A comparison of the Gaussian and ADPIC plume-depletion factors over agricultural land for 0.3-μm diameter particles for both F and B Pasquill stability categories is illustrated in Fig. A-1. A release height of 10 m and a deposition velocity of 0.002 m/s were chosen.

Both codes agree to within 10% of each other, out to a distance of 35 km. This small difference in the rate of depletion is due to the fact that the codes compute vertical diffusivities and surface deposition differently. ADPIC uses a vertical K_z profile for the diffusivity and the downward-flux gradient near the surface for the surface deposition. No vertical lid was imposed in the calculations.

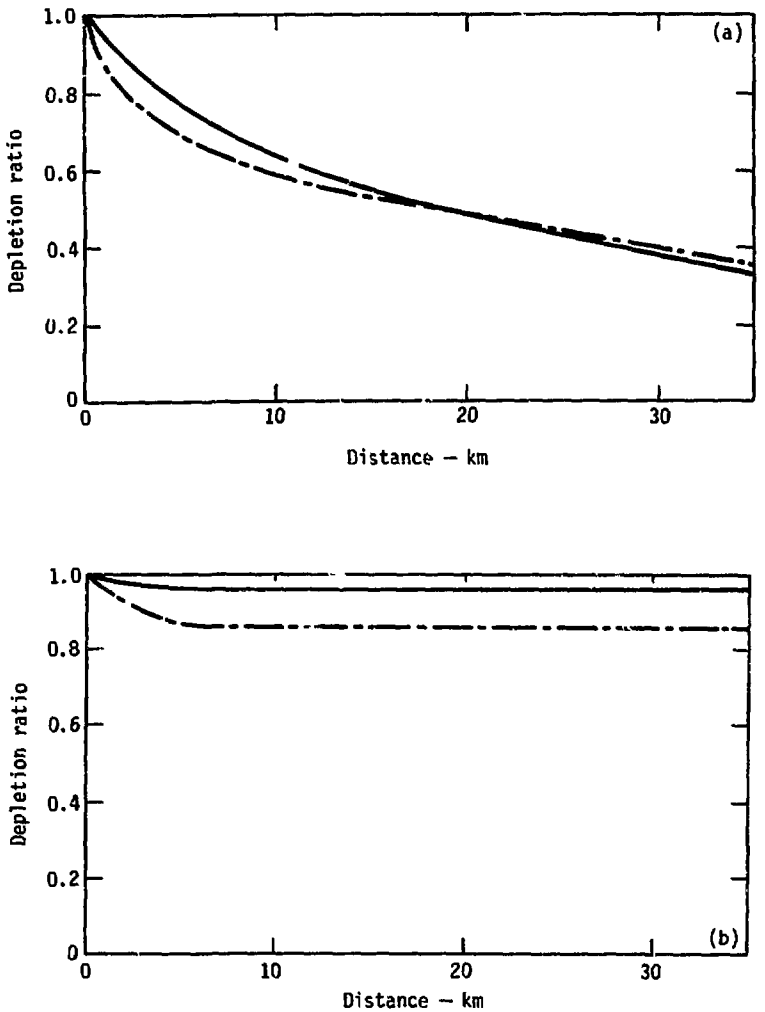

Fig. A-1. Gaussian (solid line) and ADPIC (dot-dashed line) plume-depletion factors over agricultural land for 0.3-μm diameter particles, a release height of 10 m, and a deposition velocity of 0.002 m/s: (a) F stability, (b) B stability.

Appendix B: Input Meteorological Parameters

Input Meteorological Parameters: Hudson River Valley.

Hours (EST)	Inversion Height (m)	Thermal Stability	Exponent Wind Power Law	Wind: Mesh Top (degrees)	Stations[a] (direction/speed - m/s)								
					WPT	IOI	PSK	SHP	TVT	BOP	HRO	HEM	TAR
					450[b]	20[b]	20[b]	20[b]	20[b]	20[b]	20[b]	20[b]	20[b]
18	20	4	0.17	185/2.5	270/0.95	270/0.05	040/0.35	040/0.35	100/0.25	150/2.5	170/2.5	290/1.5	180/2.5
19	30	6	0.1	185/2.4	360/0.25	320/0.25	040/0.5	040/0.35	030/0.35	150/1.5	170/1.5	295/1.8	180/1.8
20	40	6	0.1	190/2.25	360/0.5	320/0.5	040/0.75	040/0.75	030/0.5	330/0.5	170/0.5	295/1.5	180/1.5
21	50	6	0.1	190/2.12	360/0.75	320/0.75	040/1.0	040/1.0	030/0.75	330/0.75	340/0.5	300/1.5	180/1.0
22	60	6	0.1	195/2.0	360/1.0	320/1.0	040/1.25	040/1.25	030/1.0	330/1.0	340/1.0	320/1.5	360/1.5
23	70	6	0.1	195/1.9	360/1.25	320/1.25	040/1.5	040/1.5	030/1.25	330/1.25	340/1.25	320/1.8	360/1.0
24	80	6	0.1	200/1.8	360/1.5	320/1.5	040/1.8	040/1.8	030/1.5	330/1.5	340/1.5	320/1.8	360/1.5
1	90	6	0.1	205/1.65	360/1.75	320/1.75	040/2.0	040/2.0	030/1.75	330/1.75	340/1.75	360/1.8	360/1.8
2	100	6	0.1	210/1.5	360/2.0	320/2.0	040/2.25	040/2.25	030/2.0	330/2.0	340/2.0	020/2.0	360/2.0
3	110	6	0.1	215/1.4	360/2.25	320/2.25	040/2.5	040/2.25	030/2.25	330/2.25	340/2.25	020/2.25	360/2.25
4	120	6	0.1	215/1.25	360/2.5	320/2.5	040/2.5	040/2.5	030/2.5	330/2.0	350/2.0	030/2.5	360/2.5
5	120	6	0.1	215/1.25	360/2.5	320/2.5	040/2.5	040/2.5	030/2.5	330/2.0	350/2.0	030/2.5	360/2.0
6	120	6	0.1	215/1.25	360/2.25	320/2.25	040/2.25	040/2.25	030/2.0	330/1.25	350/1.25	030/2.25	360/1.25
7	120	6	0.1	215/1.25	360/2.0	320/2.0	040/2.0	040/2.0	030/1.25	330/1.0	350/1.0	030/1.75	360/0.9
8	120	6	0.1	215/1.25	360/1.5	320/1.5	040/1.25	040/1.25	030/1.0	330/0.8	350/0.8	030/1.25	360/0.5
9	120	6	0.1	200/2.0	360/1.0	320/1.0	040/0.75	040/0.5	030/0.6	330/0.75	350/0.75	100/0.25	360/0.5
10	120	5	0.17	190/2.5	180/0.5	320/0.5	180/0.5	020/0.2	030/0.2	330/0.5	340/0.5	120/0.75	360/0.35
11	280	4	0.15	180/2.5	160/0.5	140/0.5	220/2.75	210/1.75	200/2.2	150/2.0	170/2.0	150/2.75	180/2.25
12	320	3	0.12	180/2.5	180/2.4	140/2.5	220/3.1	220/3.0	210/3.0	150/3.0	160/3.0	180/2.75	180/3.0
13	360	2	0.11	180/2.5	180/3.0	140/3.0	220/3.5	220/3.5	210/3.5	150/3.6	160/3.7	180/3.8	180/3.9
14	400	2	0.08	180/2.5	180/3.25	140/3.25	220/3.8	220/4.0	210/3.75	150/3.8	160/3.8	190/3.8	180/3.9
15	400	2	0.08	180/2.5	180/3.5	140/3.5	220/3.6	220/3.8	210/3.8	150/3.8	160/3.8	210/3.8	180/3.9
16	400	2	0.08	180/2.5	180/3.5	140/3.5	220/3.5	220/3.5	210/3.5	150/3.6	160/3.7	190/3.8	180/3.9
17	400	2	0.12	180/2.5	180/2.5	140/2.8	220/2.75	220/2.75	210/2.75	150/2.75	160/2.75	230/2.0	180/2.75

[a] WPT = West Point; IOI = Iona Island; PSK = Peekskill; SHP = Ship; TVT = Indian Point; BOP = Bowline Point; HRO = Hudson River; HEM = Hempstead; TAR = Tarrytown.

[b] Observation height in metres.

Input Meteorological Parameters: Southeastern U.S.

Hours (EST)	Inversion Height (m)	Thermal Stability	Exponent Wind Power Law	Wind (Mesh Top)	Wind Speed (m/s)	Stations[a] (direction/speed m/s)														
						TV	A	C	D2	F	H	K	P	MCN	SAV	ASD	CAE	FLO	SPA	AGS
				300[b]	(m/s)	91[b]	61[b]	61[b]	61[b]	61[b]	61[b]	61[b]	61[b]	6[b]	6[b]	6[b]	6[b]	6[b]	6[b]	6[b]
18	900	2	0.05	200/4.5	3.4	190	200	200	200	200	200	190	180	200	140	120	190	190	120	200
19	20	2	0.10	200/4.75	2.7	200	200	200	200	200	200	200	190	200	140	120	190	190	120	200
20	30	3	0.17	200/5.0	2.3	200	200	200	200	270	200	200	190	200	140	120	190	190	120	200
21	35	4	0.24	200/4.75	2.3	210	200	200	070	200	200	200	190	200	320	300	270	270	300	270
22	40	5	0.28	200/4.5	2.0	210	270	140	010	140	200	270	220	200	320	300	340	340	300	310
23	45	5	0.3	200/4.25	1.8	210	290	120	010	120	200	300	220	350	320	300	340	340	300	310
24	50	6	0.3	200/4.0	1.7	220	310	100	360	100	200	300	220	350	320	300	340	340	300	310
1	55	6	0.3	200/3.75	1.6	220	340	090	360	090	200	300	240	350	320	300	340	340	300	310
2	60	6	0.3	200/3.5	1.5	220	340	090	360	090	300	300	240	350	320	300	340	340	300	310
3	65	6	0.3	200/3.25	1.4	220	330	110	340	110	200	330	240	350	320	300	340	340	300	310
4	70	6	0.3	200/3.0	1.5	220	330	110	330	110	200	330	240	350	320	300	340	340	300	310
5	70	6	0.3	200/2.75	1.5	220	330	110	330	110	200	330	240	350	320	300	340	340	300	310
6	70	6	0.3	200/2.5	1.5	220	330	110	330	110	200	330	240	350	320	300	340	340	300	310
7	70	6	0.3	200/2.25	1.9	220	330	110	330	110	200	330	240	350	320	300	340	340	300	310
8	70	6	0.3	200/2.0	2.7	220	330	110	330	110	200	330	240	350	320	300	340	340	300	310
9	100	3	0.2	200/2.25	3.4	220	090	150	045	150	200	090	030	090	140	120	160	160	120	090
10	300	3	0.18	200/2.5	3.6	210	110	180	090	180	200	150	050	150	140	120	170	170	120	120
11	600	3	0.16	200/2.75	3.9	210	130	180	120	180	200	180	090	180	140	120	180	180	120	150
12	900	2	0.14	200/3.0	4.3	200	150	190	140	190	200	190	120	200	140	120	190	190	120	180
13	900	2	0.12	200/3.25	4.4	200	170	190	140	190	200	190	150	200	140	120	190	190	120	200
14	900	2	0.10	200/3.5	4.5	190	180	200	180	200	200	190	180	200	140	120	190	190	120	200
15	900	2	0.08	200/3.75	4.6	180	190	200	180	200	200	190	180	200	140	120	190	190	120	200
16	900	2	0.06	200/4.0	4.4	180	200	200	190	200	200	190	180	200	140	120	190	190	120	200
17	900	2	0.05	200/4.25	4.0	180	200	200	200	200	200	190	180	200	140	120	190	190	120	200

[a] TV = Augusta, GA TV tower; A, C, D2, F, H, K, P = Site meteorological towers; MCN = Macon, GA; SAV = Savannah, GA; ASD = Anderson, S.C.; CAE = Columbia, S.C.; FLO = Florence, S.C.; SPA = Spartanburg, S.C.; AGS = Augusta, GA.

[b] Observation height in metres.

☆U.S. GOVERNMENT PRINTING OFFICE: 1976—689-009/7921